

APPENDIX A – TOMOGRAPHIC INVERSION

FULL WAVEFIELD ARRIVAL IDENTIFICATION

The initial stage in the direct arrival travel time inversion is the identification of the proper arrival, which represents the direct raypath from the source to the receiver. Figure 1 is a full wavefield illustration of a common receiver gather where time is along the vertical axis and receiver depth is along the horizontal. An estimate of the approximate time that the *P*-wave direct arrival energy will be recorded can be calculated knowing the spacing between the two wells and an average formation velocity of the earth media between receiver/source pair. Once the direct arrival is isolated, normal moveout can be followed down the flanks of the entire gather. Several techniques have been developed to maintain phase consistency in the picking of the tens of thousands of traces that are typical in the tomographic data set. This is accomplished by using two other gather domains by which to view the traces. Figure 2 illustrates the two additional domains beyond the familiar source and receiver gathers, where the direct arrival will exhibit unique move-out resulting in a consistent direct arrival picking position: (a) Common receiver – hyperbolic move-out (b) Common source – hyperbolic moveout (c) Common offset – linear moveout (d) Common mid-depth – 2 x hyperbolic move-out.

Principle

The basic idea behind the current tomographic approach is integrated 3-D interwell modeling. A model parameterization of discontinuous-vertical-layering with a simple two-dimensional Chebyshev polynomial representation for surfaces and velocities is employed. The model formulation is consistent with the expected vertical and horizontal resolution available in crosswell data. As a result, the tomographic problem has many fewer unknowns than the conventional pixel-based technique and is better conditioned. A further advantage of this type of model parameterization is that complex geometries like steep structural dips and “out-of-plane” well deviations can be easily handled. Furthermore, multiple crosswell data sets can be applied simultaneously to the resolution of a single 3-D velocity model.

The model formulation and forward modeling of traveltimes (ray tracing) are described first. Then, the traveltimes inversion and the application of the continuation strategy to smoothing constraints for the 3-D parameterization—an approach to regularization that greatly improves resolution—is explained.

The characteristics of the algorithm are described in more detail in the following paragraphs.

Model Description

The model consists of two parts; a structural part made of vertically-discontinuous layers that mimic geologic contours, and a functional part that, for traveltimes tomography, is used to represent slowness (reciprocal velocity). Both the structural part (surfaces) and the functional part (subsurface parameters) are specified by Chebyshev polynomials.

Figure 3 is a schematic showing a vertical slice through the 3-D model parameterization. Each of the surfaces $Z_i(x,y)$ is represented by a 3rd order 2-D Chebyshev polynomial. The slowness within each layer (bounded by a surface above and below) is specified with a similar 2-D Chebyshev polynomial, $S_i(x,y)$. This type of stratification is typically more “earth-like” and has been demonstrated to provide vertical resolution comparable to the scale of wireline logs. Further, the polynomials can represent velocity varying laterally in two dimensions with relatively few parameters. The combination allows the specification of velocity, and other quantities of interest, anywhere within a particular 3-D volume. Hence the ability to obtain estimates of 3-D velocity fields from multiple profile crosswell data.

The 2-D Chebyshev polynomials are a limited tensor product of 1-D Chebyshev polynomials, keeping only terms of up to 3rd order. Equation 1 shows the form of the polynomials.

$$\begin{aligned}
 F(x, y) = & \\
 & + C_0 \\
 & + C_1x + C_2y \\
 & + C_3xy + C_4(2x^2 - 1) + C_5(2y^2 - 1) \\
 & + C_6(2x^2 - 1)y + C_7(2y^2 - 1)x + C_8(4x^3 - 3x) + C_9(4y^3 - 3y)
 \end{aligned}
 \tag{Eq. 1}$$

The coefficients C_0 through C_9 weight the contributions of the orders of the polynomial. There is a constant term (C_0), two first-order terms (C_1 and C_2), three second-order terms (C_3 through C_5) and four third-order terms (C_6 through C_9). By weighting the coefficients it is possible to fit surfaces of varying spatial smoothness. These ten coefficients provide essentially cubic variability in structure and velocities. While certainly insufficient to represent some scales of geologic heterogeneity, a large class of real world crosswell problems can be adequately treated with this representation.

The structural part of the model is constrained to be geologically realistic by fitting the surfaces to horizon picks from wireline log correlations in the wells. The coefficients for the Chebyshev polynomials are found by singular value decomposition of this data. Figure 4 shows a real example of different order surfaces fit to horizon picks from a series of five deviated wells in Chevron's Buena Vista Hills field in Kern County, California (Langan, et al., 1998). The horizon picks from wireline logs are shown as colored cubes in Figure 4a. Zero-order surfaces are horizontal and would be used only in the absence of *a priori* geologic or well-log information about structure. First-order surfaces are constant dip and plunge planes, appropriate when there is limited well-log information available (Figure 4b). Second- and third-order surfaces are appropriate when there exists *a priori* information from a number of neighboring wells in areas of structural complexity, as in Figures 4c and 4d.

The model used for tomography is obtained by interpolating the initial surfaces to a nominal vertical spacing of less than one meter. Figure 5 demonstrates an elevation view of a series of surfaces in the vicinity of a pair of deviated wells that for clarity have been interpolated to the coarser nominal spacing of 7.5 m. After this initial interpolation of the *a priori* "horizon pick" surfaces, the structural part of the model remains unchanged throughout the traveltimes inversion procedure; only the velocities in the layers between the structural surfaces can change.

Traveltimes Calculation and Ray Tracing

The type of ray tracing used in crosswell tomography has been studied extensively. Iterative solutions to the tomographic problem require ray tracing for accuracy, particularly when strong velocity inhomogeneities are present. Although the "shooting method"—propagation of rays by successive application of Snell's law at interfaces or cell boundaries—has widespread use, high wavenumber fluctuations in velocity can cause it to fail. In addition, the computational overhead to obtain accurate raypaths through high vertical resolution models is large even in 2-D, and for 3-D becomes prohibitively expensive.

The "bending method", in contrast, is a fast two-point perturbative approach that relies on Fermat's principle of least time. The two point method can provide solutions where a propagator method can fail. Another clear advantage of the bending method is that it can be expected to operate much faster than the shooting method for 3-D problems. For these reasons we employ the bending method.

The use of Chebyshev polynomials for the model parameterization introduces algorithmic advantages for the ray tracing because we can analytically calculate traveltime and derivatives. Furthermore, the individual polynomials are laterally continuously differentiable throughout the model, and the small number of parameters required improves the stability and robustness of both the forward problem (ray tracing) and the inverse problem (velocity inversion).

There are two assumptions involved in the forward modeling and traveltime calculation:

Slowness within a layer is a function of x and y , but invariant of z .

Raypaths are straight lines between layer boundaries.

These assumptions hold to first order because layer spacing is chosen small compared to wavelength for most crosswell data. The traveltime integral for a single layer is given by Equation 2, and the solution can be simply calculated in parametric form. The corresponding geometry is shown in Figure 6.

$$t = \int_A^B S(x, y) dl \quad \text{Eq. 2}$$

where t is the traveltime, $S(x,y)$ is the polynomial slowness within the layer, A and B are the intersection locations of the raypath with the surfaces that bound the layer, and dl is a differential element of length along the path from A to B . The total traveltime for a ray intersecting many layers is given by the sum over the individual segments.

To ray trace with the bending method, we start with the straight ray connecting source and receiver, and minimize traveltime by iteratively finding perturbations to the raypath. Due to the vertical stratification of the model, z on the surfaces is a function of x and y , and the dimensionality of the problem is reduced to solving only for the updates to x and y at the intersections of the raypath with the surfaces.

Using Newton's method to solve the nonlinear ray tracing problem yields an elegant structure for the successive linearized problems. According to Fermat's principle, the ray with the minimum traveltime arrives first. Thus to compute first arrivals, the objective function that we minimize is traveltime, and derivatives of this functional with respect to the intersection locations can be determined in closed form. These partials only involve terms from adjacent layers, and the Hessian matrix of second derivatives is therefore band-diagonal and symmetric with nonzero elements in only three super-diagonals. The linear systems are quickly solved using matrix decomposition or factorization.

Figure 7 shows rays calculated by the ray tracer in a finely layered media (based on the interpolation of sonic logs) with lateral variation inside the layers. Notice the stability and good linking properties of the ray tracer, in particular for raypaths closer to the horizontal, where ray bending is more severe. As shown in the figure, rays corresponding to reflected arrivals can also be traced.

Velocity Inversion and the Continuation Strategy

A simple definition of tomography is the reconstruction of a field from line integrals through the field. These line integrals for traveltime tomography (raypaths) are non-linear with respect to the field we seek to reconstruct (velocity distribution). Therefore tomography algorithms linearize the problem around a background velocity and iteratively seek updates to the velocity. For a particular source and receiver geometry and velocity parameterization, traveltimes are modeled by computing line integrals through the velocity field. Then a system of equations is solved that relates the sensitivity of traveltime with respect to changes in the velocity parameterization (Fréchet derivatives) to the predicted error of the modeled traveltimes.

In our formulation of the linear system for traveltime inversion, we exploit the analytic form of the expression for traveltime in the calculation of the Fréchet derivatives. In each layer we have to solve for ten coefficients, which is fewer parameters than we need for a convenient pixelized or gridded model with equivalent lateral resolution. Although the choice to use Chebyshev polynomials results in fewer model parameters and thus a more well-conditioned inverse, using polynomials requires that some type of regularization be applied within the inversion scheme in order to avoid extreme variations in velocity in areas of the model that have poor ray coverage.

While some type of constraints is necessary, care must be exercised in choosing the proper implementation, because the regularization will overprint inversion results. Certainly some of the “regularization overprint”, which in general amounts to smoothing, may be preferable to the alternative: high-wavenumber fluctuations in velocities. However, we should exercise care in order to achieve the maximum resolution that can be obtained from the traveltime data. This implies using the minimum constraints that are required to stabilize the problem.

The effect of employing regularization is to change an ill-posed problem into a “nearby well-posed problem”. The difficulty is to implement regularization such that the solution to the “nearby” problem remains very nearly a solution to the original problem. Bube and Langan (1994) solve separate iterative non-linear problems for fixed regularization, successively decreasing the level of the constraints until the data, not the regularization, is in control. They call this “smoothing constraints with a continuation strategy”, and refer to each of the fixed regularization problems as a “continuation step”. The key idea they present is to use the final solution from the previous “step” (fixed regularization problem) as the initial model for the iterative solution to the next, less regularized, problem.

To apply the smoothing constraints to the common earth model introduced here, vertical or horizontal smoothness is achieved by forcing the appropriate derivative of slowness to be small. Vertical smoothness is applied using numerical differences of polynomial coefficients in adjacent layers, and horizontal smoothness can be applied by directly constraining the polynomial coefficients in closed form. For the crosswell 3-D problem we apply two horizontal penalties, one for derivatives along the interwell plane (tangential), and one for derivatives perpendicular to the interwell plane (normal). Application of the horizontal penalties prevents extreme variations in velocity in areas where there is little ray coverage.

The overall continuation strategy is to reduce the penalties forcing model smoothness gradually as the inversion process proceeds. In general, the fixed iterative non-linear problem in each continuation step is considered “solved” when the objective function has reached a minimum for that level of regularization. Usually it requires more non-linear iterations to reach a minimum when the regularization is weak. Ultimately the penalties can be made very small, and the data itself will control the inversion results. Further, we understand the physical correlation of regularization for the continuation approach. Where there is no data controlling the values of model parameters (the “null space” of the traveltime problem), the penalties force the model to be smooth.

Data Selection

It is a common feature of most crosswell data sets acquired in generally horizontally stratified media that the recorded waveforms have a complicated appearance for source-receiver pairs corresponding to horizontal, or near horizontal, raypaths. This is illustrated in Figure 8, which shows a common-source gather from a crosswell data set collected in a West Texas carbonate formation which exhibited a large velocity contrast at the formation boundaries. Notice that, although the direct arrival can be easily and unambiguously followed for the larger source-to-receiver depth separations (direct-arrival flanks), event identification is very difficult for the near-horizontal directions (within 20 degrees from the horizontal approximately). This happens because, for these directions, a number of other strong events (head waves, guided waves, and post critical reflections) compete with the direct arrival at and around formations with

large velocity contrasts. Often, the first arrival energy from near-horizontal propagation is not a *P*-wave direct arrival but rather another wave mode, like the ones mentioned above. To avoid ambiguous picks caused by waveform complexity, we generally do not use the direct arrival traveltime picks with propagation angles close to horizontal for the inversion process. In areas where the velocity contrast between formations is less than approximately ten percent, traces at smaller angles can be reliably picked and are included in the inversion process.

Velocity Image vs. Velocity Model

The traveltime inversion may have the objectives of providing a velocity model for reflection imaging, a velocity model for interpretation of formation properties and property changes or both. In general, reflection imaging requires the best behaved/smoothest model that provides a good traveltime match. Models with inversion artifacts oftentimes produce erratic reflection traveltimes. This results because the reflection raypaths are not contained generally within the direct arrival raypaths solved for in the inversion. A smoother model that produces a consistent set of direct arrival times is typically the best model for reflection stacking and a good starting point for velocity analysis and static corrections.

If a map of formation properties is desired, we oftentimes are interested in the lateral variation of the property. A velocity “image” therefore may be provided with enhanced lateral resolution at the price of increasing inversion artifacts around the edge of the image.

Therefore, a clear definition of the objective of tomography is essential. Like most seismic velocity models, the crosswell reflection velocity model may not be the ideal information for an interpreter.

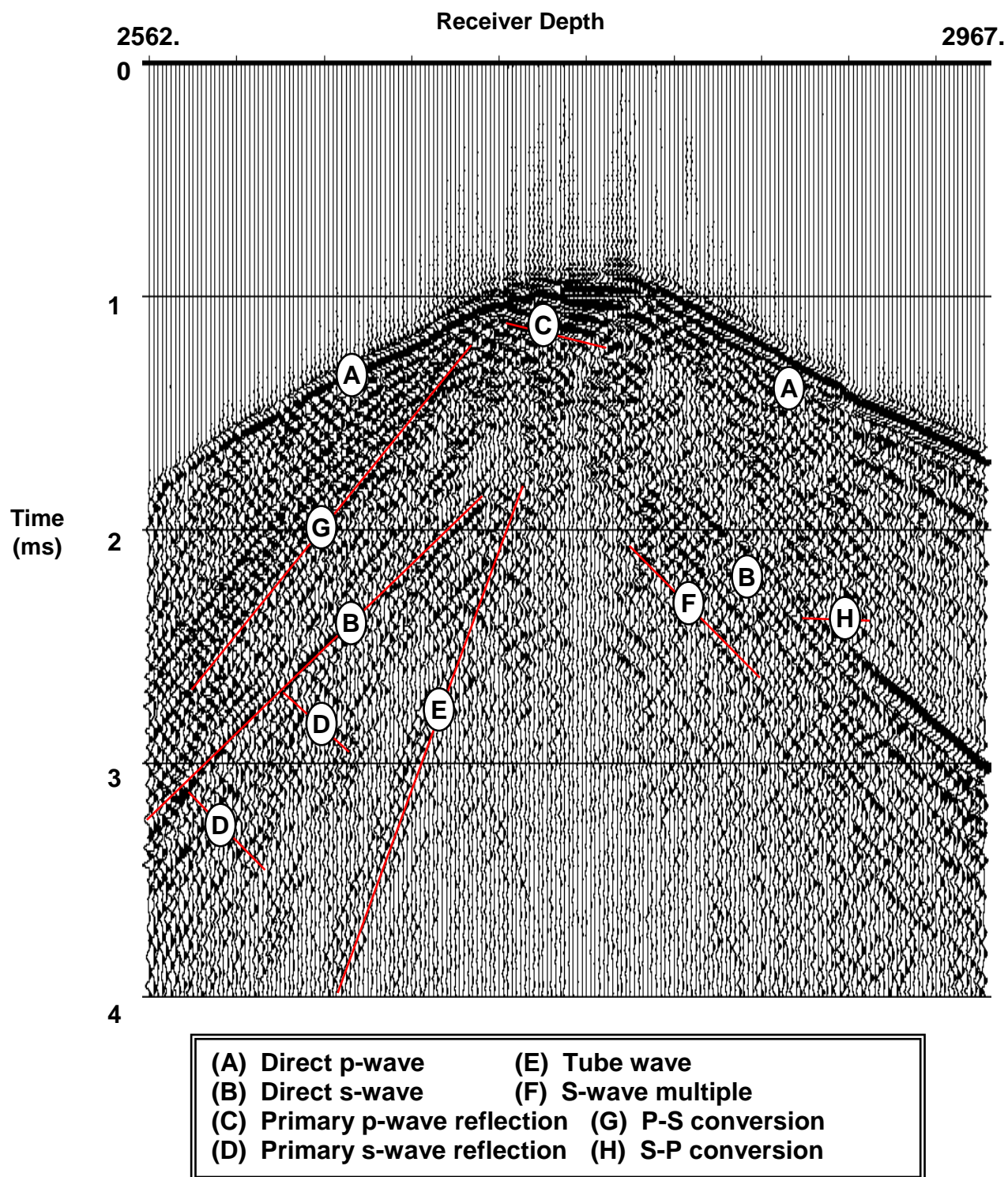


Figure 1: Arrivals identified in a crosswell common source gather.

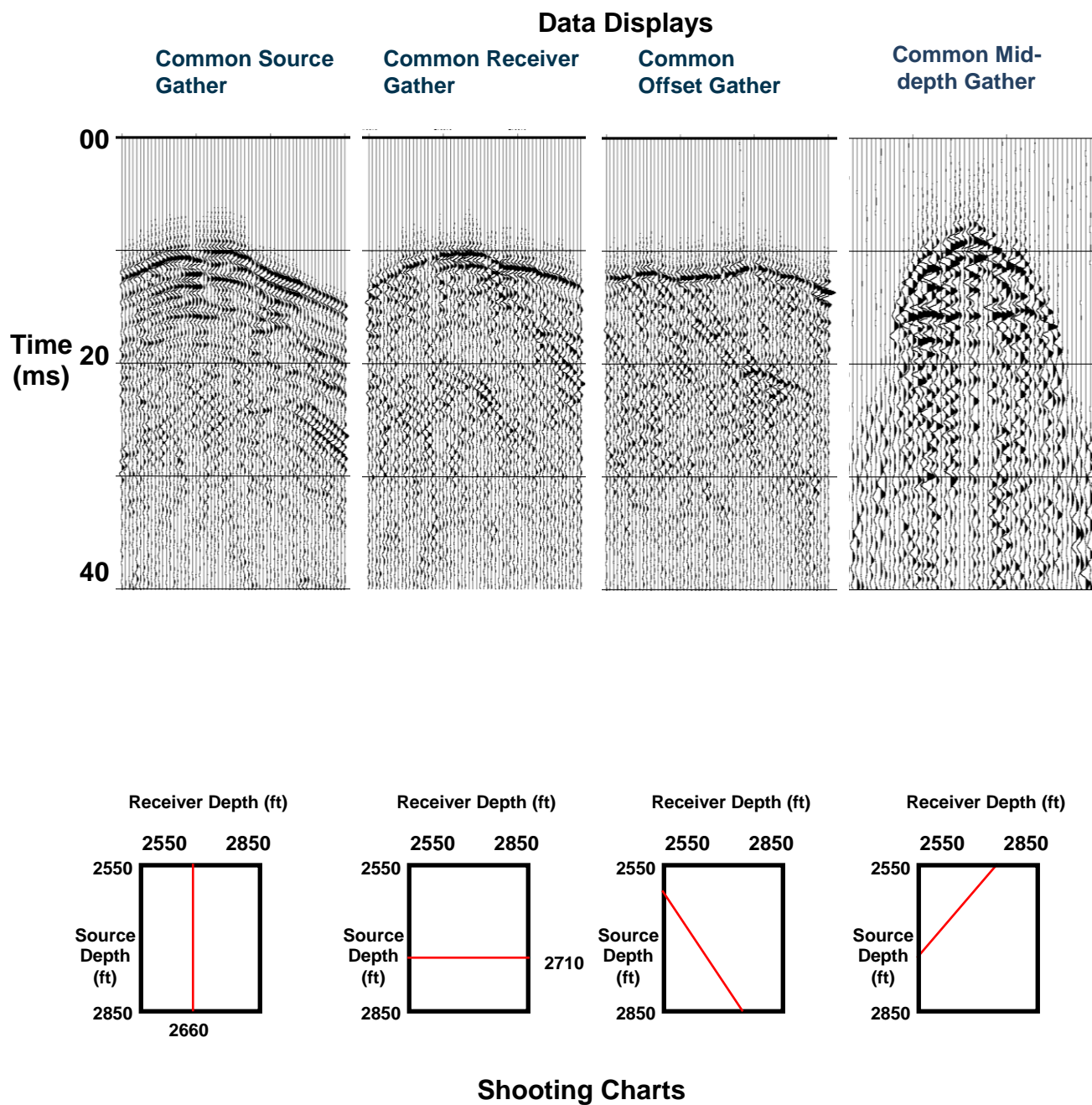


Figure 2: Four crosswell data displays from the time-domain data cube.

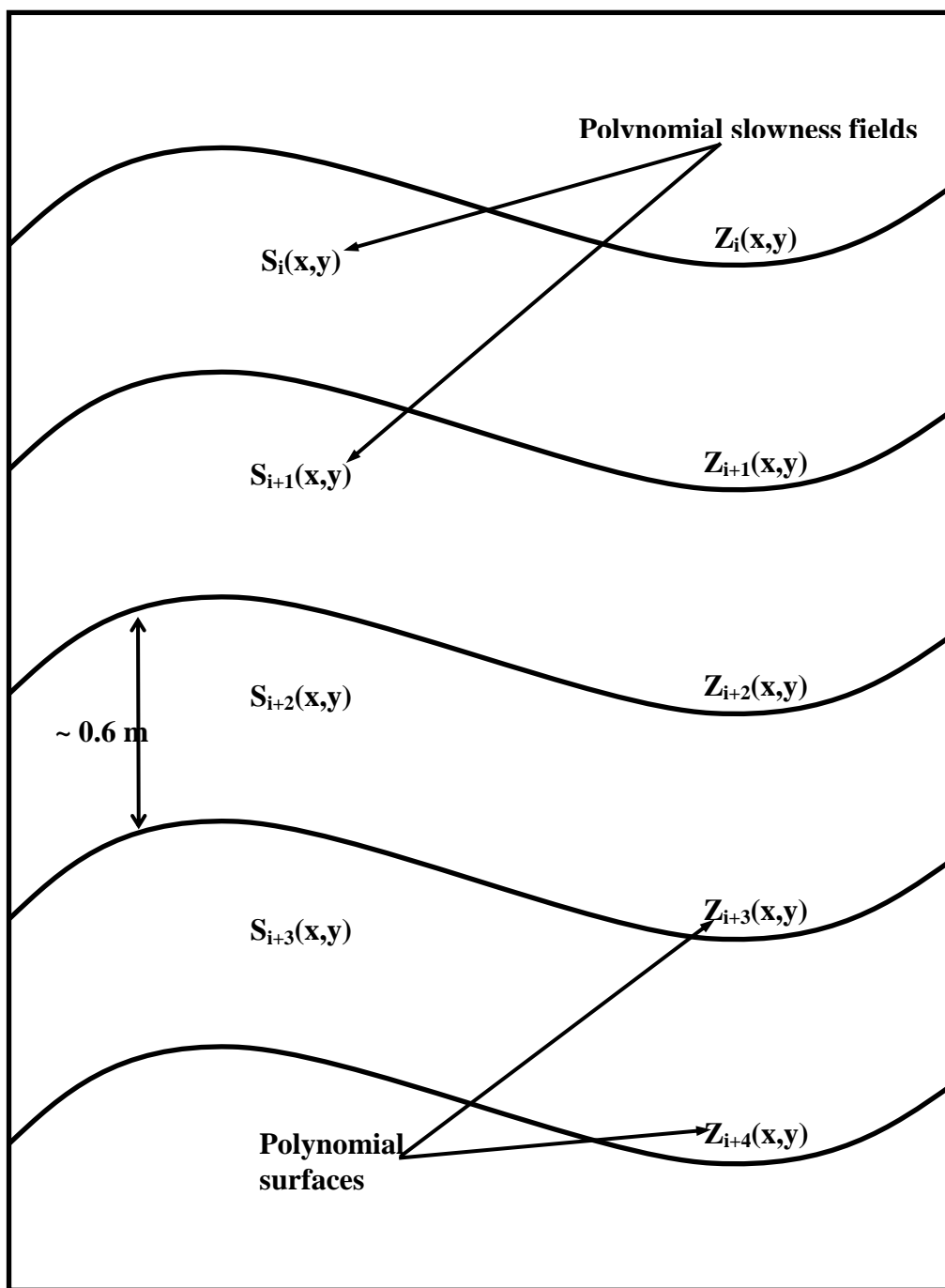


Figure 3: Schematic of common earth model geometry (vertical slice through 3-D model)

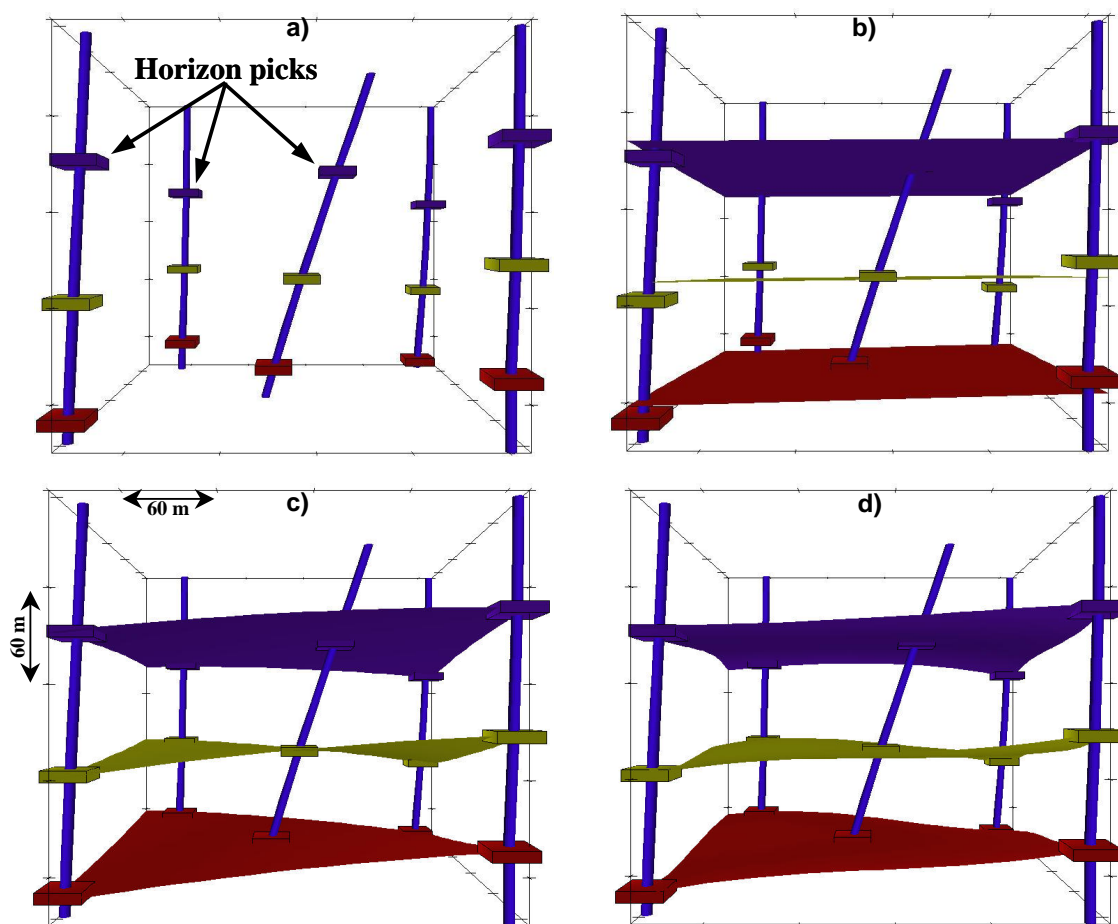


Figure 4: Chebyshev polynomial surfaces fit to horizon picks in deviated wells:

- a) horizon picks**
- b) first-order surfaces fit to horizon picks**
- c) second-order surfaces fit to horizon picks, and**
- d) third-order surfaces fit to horizon picks.**

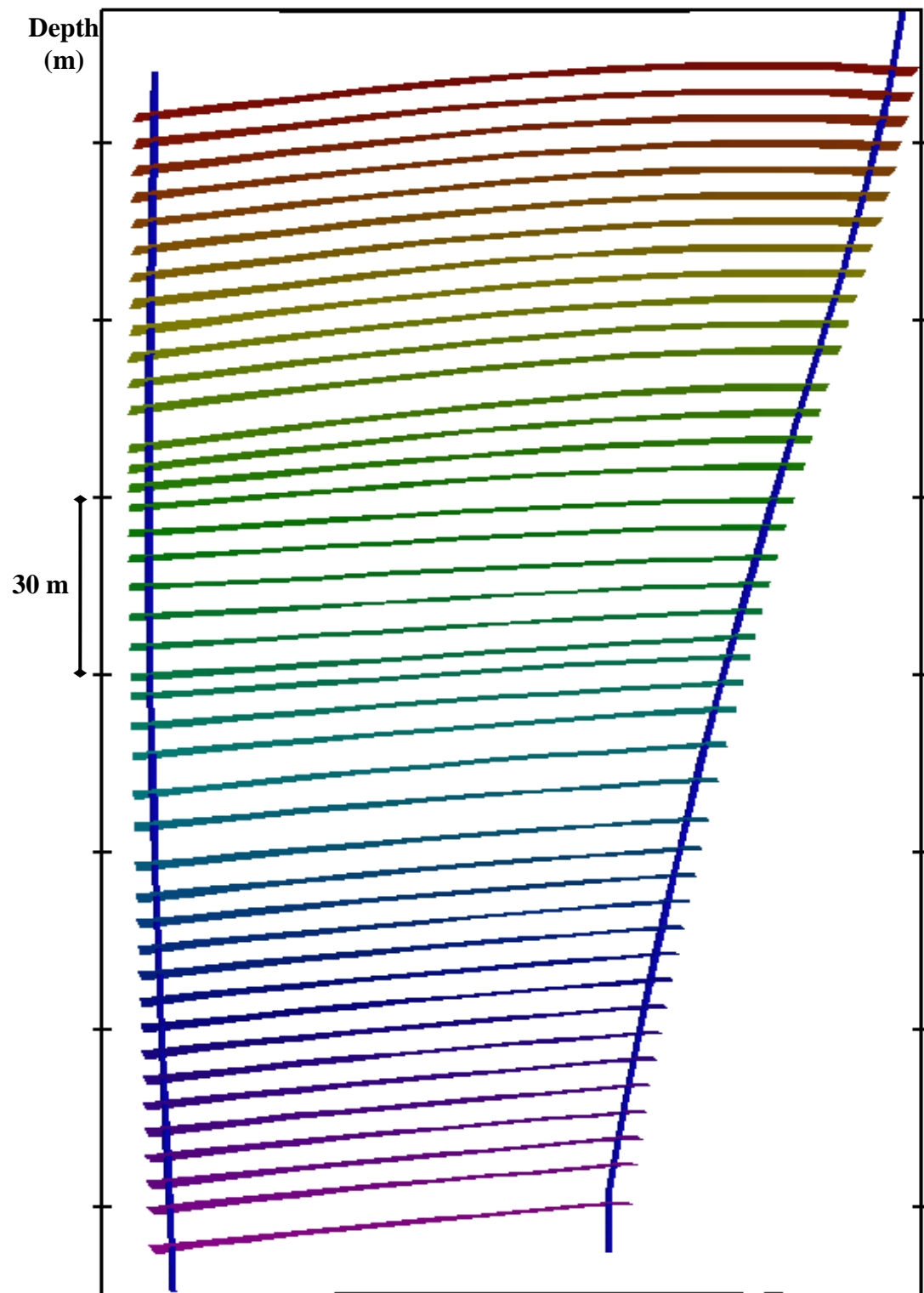


Figure 5: Elevation view of surfaces in the vicinity of a pair of deviated wells interpolated to nominal spacing of 7.5 m.

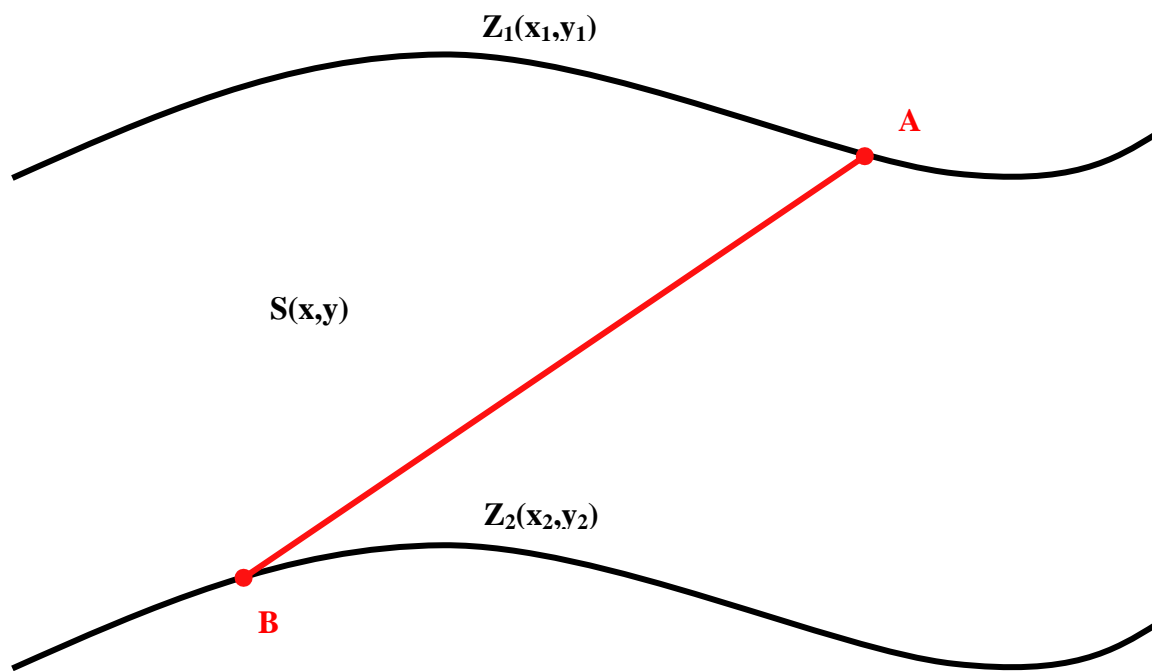


Figure 6: Schematic of geometry for traveltime calculation within a layer.

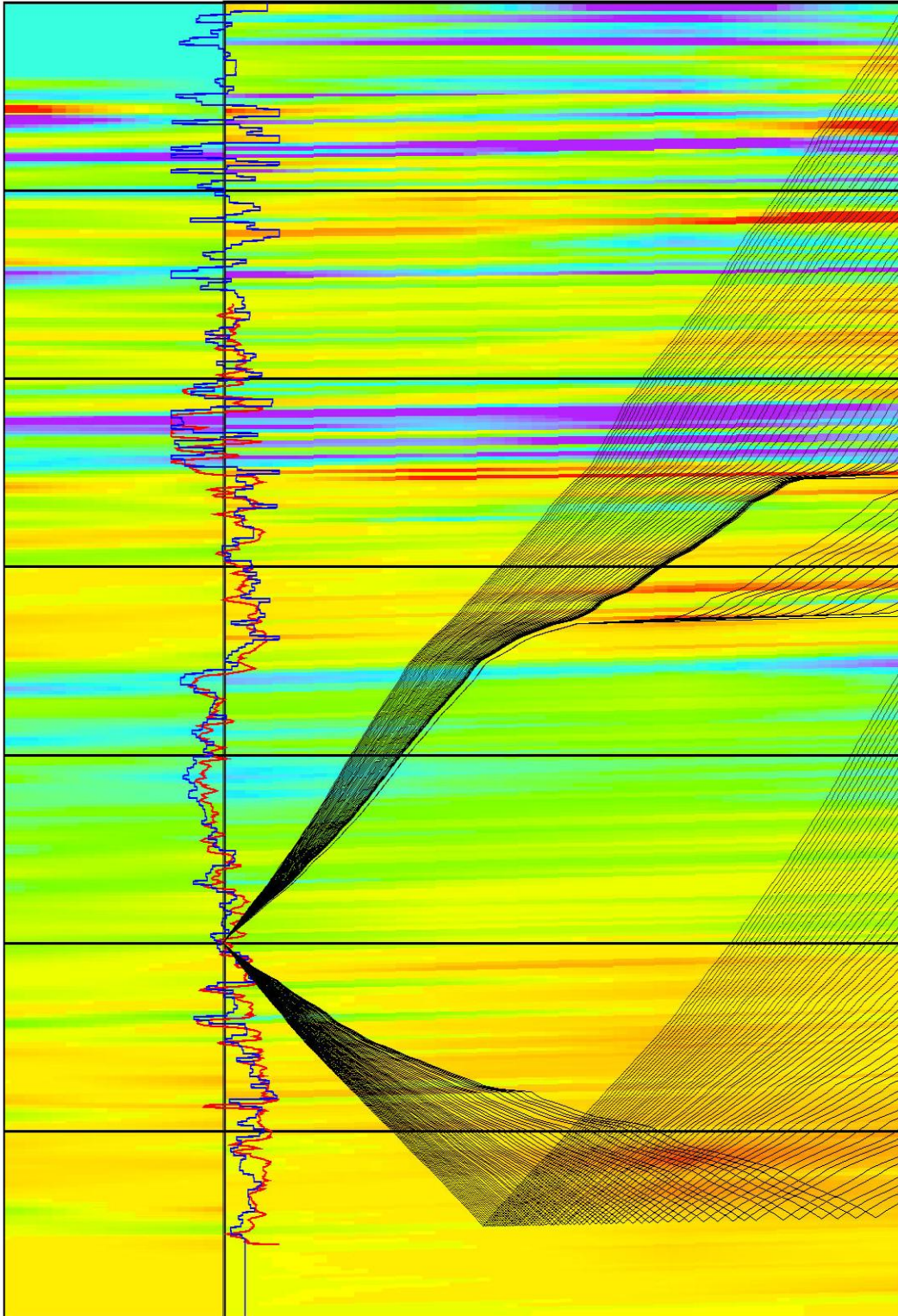


Figure 7: Example of rays calculated in a finely-layered, laterally varying medium

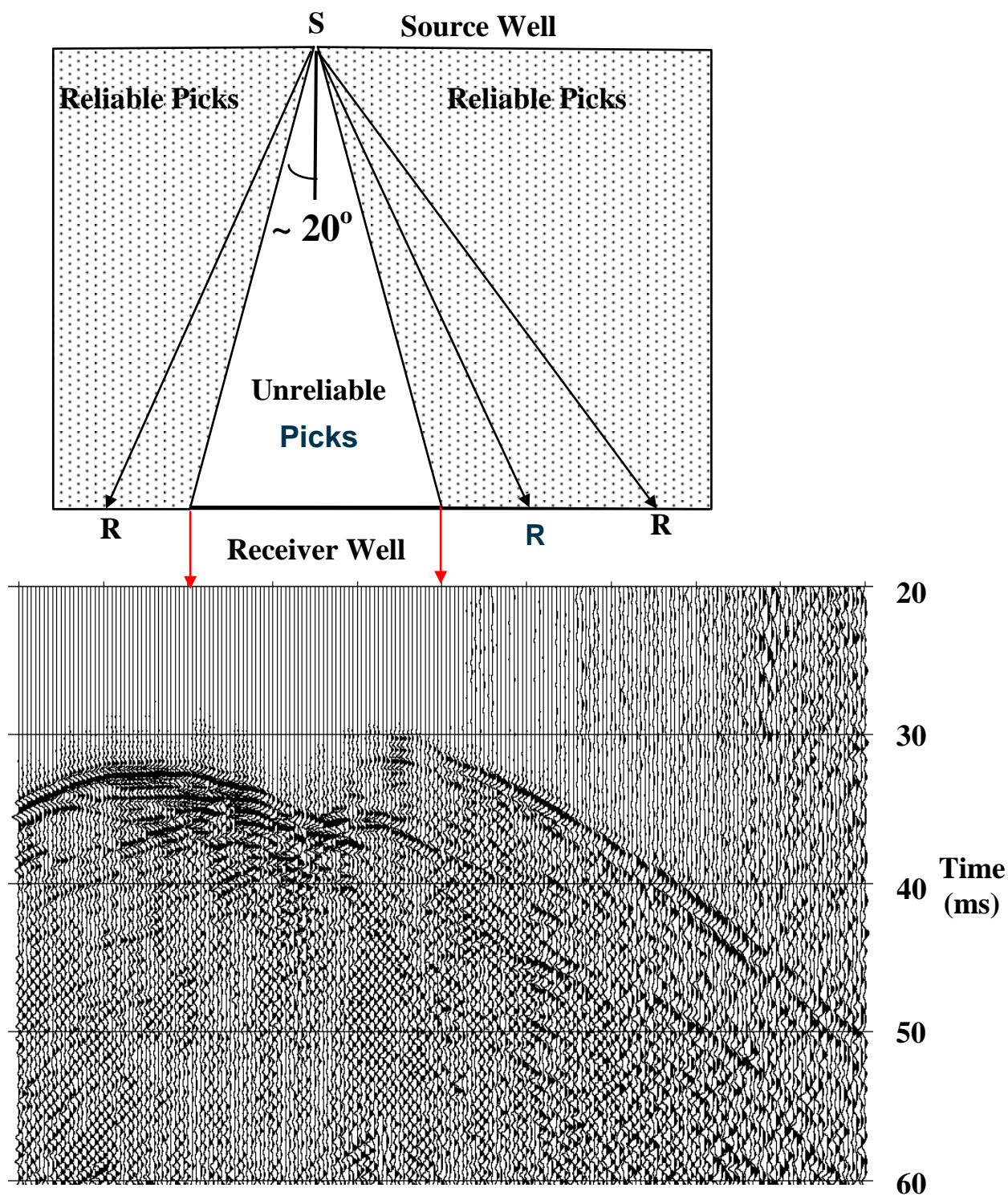


Figure 8: Crosswell common source gather and a schematic of the regions where reliable picks can be made.

Appendix B – Reflection Imaging

Introduction to Reflection Imaging

Crosswell seismic data are acquired by placing both seismic sources and receivers in wellbores close to the target of interest. Two types of information are acquired: the direct paths between source and receivers and reflection information from horizons below the source and receiver positions. In Figure 1 the direct paths, shown as solid lines, allow direct measurement of seismic velocity. An inversion procedure produces a map of seismic velocity between the intervals logged in the two wellbores, often called a tomogram. The reflection paths are shown in Figure 1 as the dotted lines. The reflection data are imaged to produce what is typically shown as a wiggle trace section, a seismic line between two wellbores.

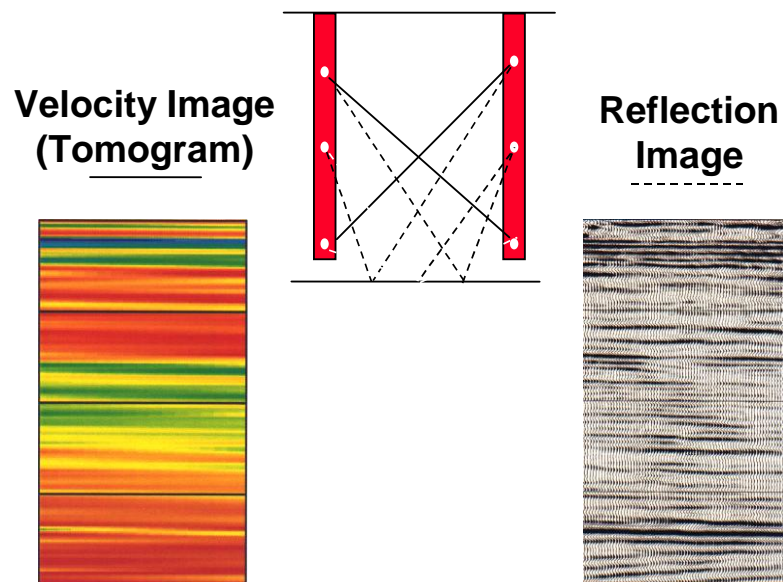


Figure 1. Typical raypaths for direct and

The general flow for crosswell seismic data processing is shown in Figure 2. The fundamental interwell information is contained in the velocity image, produced using traveltime inversion (see *Tomographic Inversion Summary Description*) and the reflection image produced using reflection imaging as described herein. One fundamental advantage of crosswell versus surface seismic and VSP, the ability to directly estimate a velocity field for reflection imaging, is exploited in the general flow. Traveltime inversion is used to produce a velocity model for reflection imaging. The remainder of this section discusses the individual steps in reflection imaging. The survey geometry, formation velocity, attenuation, structure, and imaging objective control the exact sequence of steps followed in reflection imaging. Some steps in the processing flow are fully elective; used for some data sets and not for others. In some steps a variety of methods (e.g. filters) may be selected to achieve the objective of the step. Steps such as wavefield separation may be performed selectively to remove arrivals one at a time. The selection process is detailed in the following description.

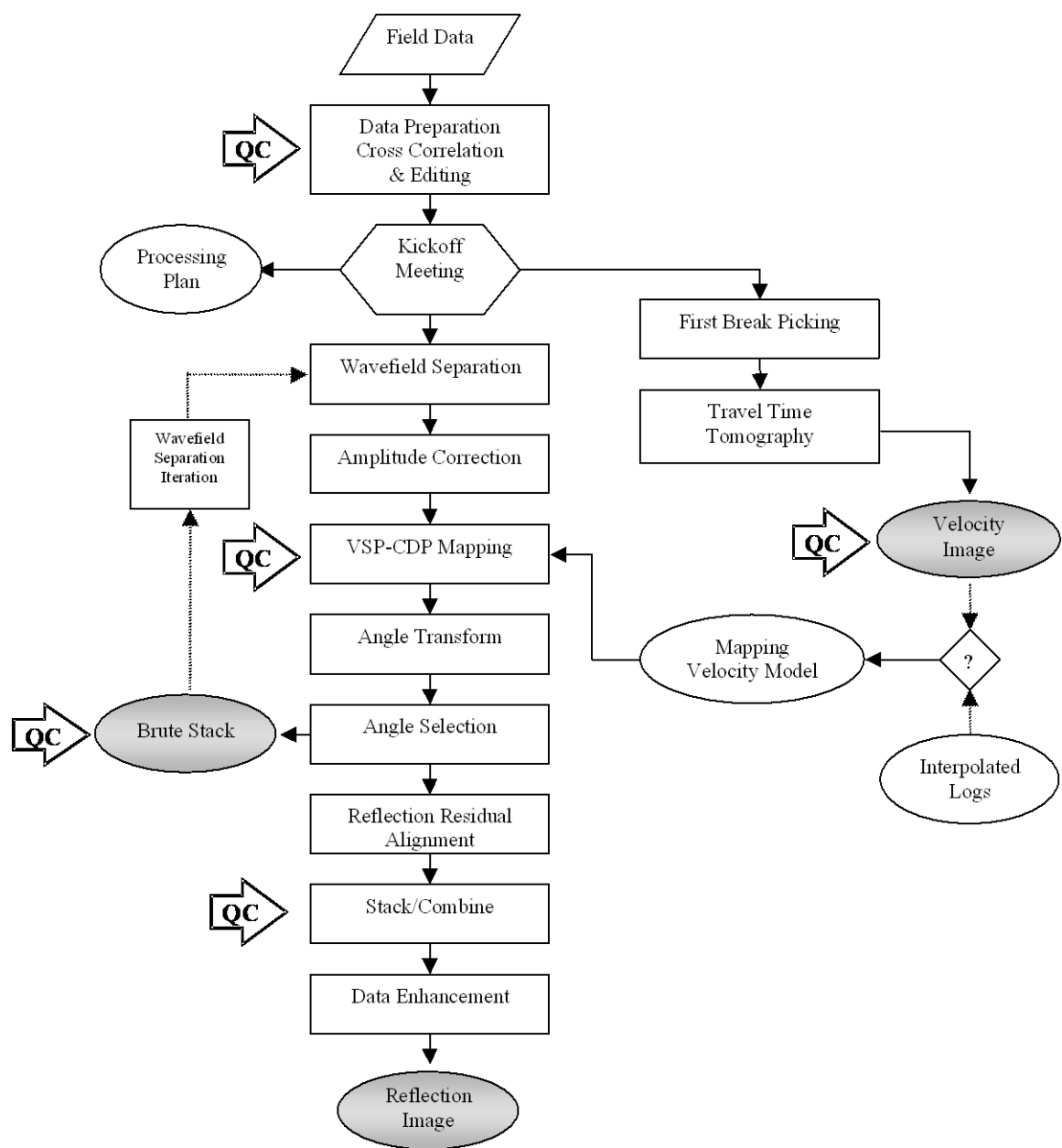


Figure 2. Data processing flow.

Pre-Processing

Processing: both direct arrival traveltime picking and reflection imaging. Variations in SNR are produced by two effects:

- Variable noise levels in the receiver well, typically from depth to depth, but occasionally from time to time during the survey
- Variable signal amplitude due to several factors including
 - ◆ Source and receiver radiation patterns
 - ◆ Formation impedance
 - ◆ Transmission/reflection coefficients

Variations in frequency content are due to variations in attenuation in different formations. Two processes are typically used in the pre-processing to equalize the data set.

- Spectral whitening – removes narrow band noise due to production field machinery, and equalizes the frequency content of the signal that is variable due to variable formation attenuation. A mild zero phase spiking deconvolution is most often used with 2 to 10 percent noise added.
- Bandpass filtering. A filter is selected with the upper cutoff set to the upper frequency limit due to formation attenuation. Spectra as a function of depth are used identify the typical upper limit of signal frequencies. The low cutoff is often times set based on SNR considerations. The spectra of noise shots (those acquired without a source firing) are compared with those from signal shots to determine the lowest frequency with acceptable SNR.

Bandpass filtering is always a part of the pre-processing. Spectral whitening is used based on the criteria given above.

Wavefield Separation

Wavefield separation refers to removing arrivals present in the crosswell data set other than the desired reflection events. The term is borrowed from vertical seismic profiling (VSP) processing. In offset VSP processing any significant amplitude arrival must be removed in wavefield separation due to the lack of stacking fold available for noise cancellation. A significant advantage in crosswell data is the high stack fold (40 to 100) available for stacking the reflection data. Stacking attenuates many of the unwanted arrivals in crosswell data. Therefore, the general wavefield separation approach is to remove only those unwanted arrivals that contribute to the noise wavefield in the stacked section. Based on processing experience, a few wave modes are always removed in wavefield separation. Other modes may be selectively removed based on their unwanted contribution to the stacked image.

Up/Down Separation

A crosswell data set contains reflections from below the source and receiver (upgoing reflections) and from above the source and receiver (downgoing reflections). Typically, because targets of interest exist near the terminal depth (TD) of the well, upgoing reflections are used in reflection imaging. A broad f - k filter is used to remove the unwanted reflection trajectories. This filter can remove a significant portion of f - k space without influencing the desired reflected energy because of the extremely different, virtually orthogonal, moveouts of upgoing and downgoing reflections. The filter is applied as two f - k filters, one to common receiver gathers and the second to common source gathers, to effectively remove a half-space within f - k space. If significant structure is present, the fan filters are rotated to align with the reflection.

Direct Arrival Removal

The direct arrival is often the largest amplitude event in a crosswell section. The direct arrival is removed by aligning to the first break traveltimes (from traveltime picking) in common offset gathers and applying a tight reject filter with filter characteristics based on direct and reflected moveouts. The filter may be a mean reject, median reject, or f - k fan reject formulation.

Tube Wave Removal

The situations where large amplitude, quasi-linear moveout tube wave (fluid borne interface waves in the wellbore, converted at diameter contrasts or formation boundaries with head waves) are observed in common source or common receiver gathers, tube wave removal filtering may be applied. In its simplest form, the data are aligned to the tube wave velocity observed in the data and a mean or median reject filter is applied with the length adjusted to preserve reflection events while maximally attenuating the tube waves. Variations in fluid velocity and tube wave propagation require different moveout velocities for different conditions. Additionally, tube wave moveouts are not linear due to local interactions in the borehole. Therefore, a static correction is often applied prior to application of the removal filter. The static correction is then removed from the data following filtering.

Reflection Trajectory Guided Filtering

In early crosswell work, wavefield separation techniques were based on the VSP experience. Crosswell data sets (typically consisting of a few hundred common receiver gathers) were processed as a collection of independent VSPs (each common receiver gather being the equivalent of one VSP experiment). Although this approach worked reasonably well for profiles with short well separation, high fold and high SNR data, it failed to produce good results for noisier profiles with long well spacing.

Trajectory guided filtering relies on a much more complete use of the crosswell data set. The main innovation is that instead of processing in a single sorting domain (common source or common receiver gathers), we now work in four domains simultaneously. The four domains are; common source and common receiver gathers (CSG and CRG), common offset (COG) and common mid depth gathers (CMG). A common offset gather is a collection of traces for which the source-receiver depth difference is constant. A common mid depth gather is shown schematically in Figure 3. If we connect source/receiver pairs in a common mid depth gather by straight lines, all the lines intersect at the same point. Figure 3 illustrates that a single common mid depth gather can image a reflector from one well to the other (the reflection points are close to the source well when the receiver is above the source and close to the receiver well when the source is above the receiver).

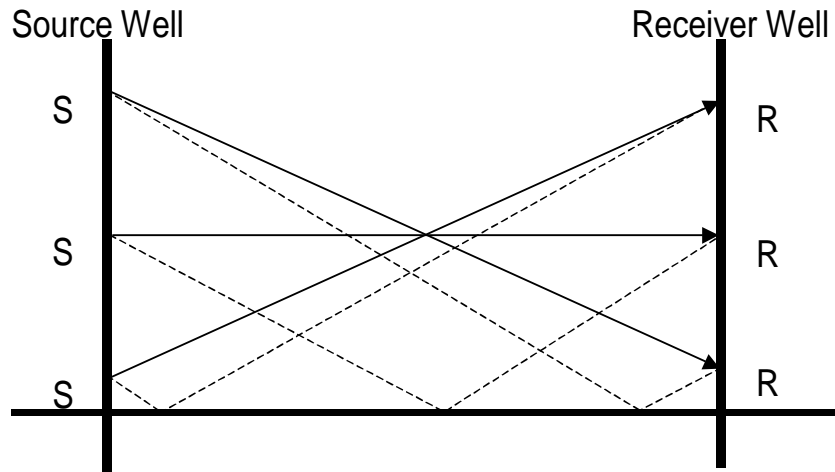


Figure 3. Schematic representation of a common mid depth gather

The basic shortcoming of other approaches is the following: either the wavefield separation filters would leave a lot of coherent noise behind, or they would hurt the reflection events themselves through aliasing. This occurred because a velocity filter designed to reject a certain noise mode that interferes with reflections in part of the gather is likely to also reject reflections in other parts of the gather.

The above discussion demonstrates that velocity filters cannot work well with crosswell data, unless their velocity passband changes rapidly to adapt to the change in slope of the reflection events across the gather resulting in signal degradation due to filter edges. Typically, this reflection trajectory guide filter mixes across traces in mid-depth gathers because in common mid depth gathers, reflection moveouts are much more similar, allowing application of a moveout correction to the gather that will align the reflection events and transform the gather to one in which all reflectors are horizontal. Because the trajectories are approximately parallel, the alignment of the events can be achieved with a minimal amount of signal distortion (stretching). This filter is not appropriated in very complex geologic structure like over-thrust or intrusion environments.

Amplitude Corrections

Three major factors influencing the amplitude or crosswell events are considered and computed in crosswell processing:

- Formation impedance
- Source and receiver radiation patterns
- Transmission effects

These quantities are computed based on the velocity model during reflection ray tracing. The exact quantities provide interesting quality control (QC) of amplitudes, but are hypersensitive to the velocity model. Therefore, we make one of the following data-driven amplitude corrections to the time traces prior to VSP-CDP imaging:

- Normalize the energy in each trace to the same level
- Normalize the direct arrival amplitude in each trace to the same level
- Isolate the energy along reflection trajectories based on the velocity model and normalize each trace based on the energy in a window corresponding approximately to incidence angles using in reflection imaging.

These corrections are progressively more correct and result in reasonable compensation for images using greater incidence angles

VSP-CDP Mapping/Reflection Ray Tracing

The VSP-CDP mapping approach used in offset VSP data processing is one imaging method used. A velocity model from the traveltimes inversion is used in tracing reflection raypaths.

Model Description

The model consists of two parts; a structural part made of vertically-discontinuous layers that mimic geologic contours, and a functional part that for traveltimes tomography is used to represent slowness (reciprocal velocity). Both the structural part (surfaces) and the functional part (subsurface parameters) are specified by Chebyshev polynomials.

Figure 4 is a schematic showing a vertical slice through the 3-D model parameterization. Each of the surfaces $Z_i(x,y)$ is represented by a 3rd order 2-D Chebyshev polynomial. The slowness within each layer (bounded by a surface above and below) is specified with a similar 2-D Chebyshev polynomial, $S_i(x,y)$. This type of stratification is typically more “earth-like”, and has been demonstrated to provide vertical resolution comparable to the scale of wireline logs. Further, the polynomials can represent velocity varying laterally in two dimensions with relatively few parameters. The combination allows the specification of velocity, and other quantities of interest, anywhere within a particular 3-D volume. Hence the ability to obtain estimates of 3-D velocity fields from multiple profile crosswell data.

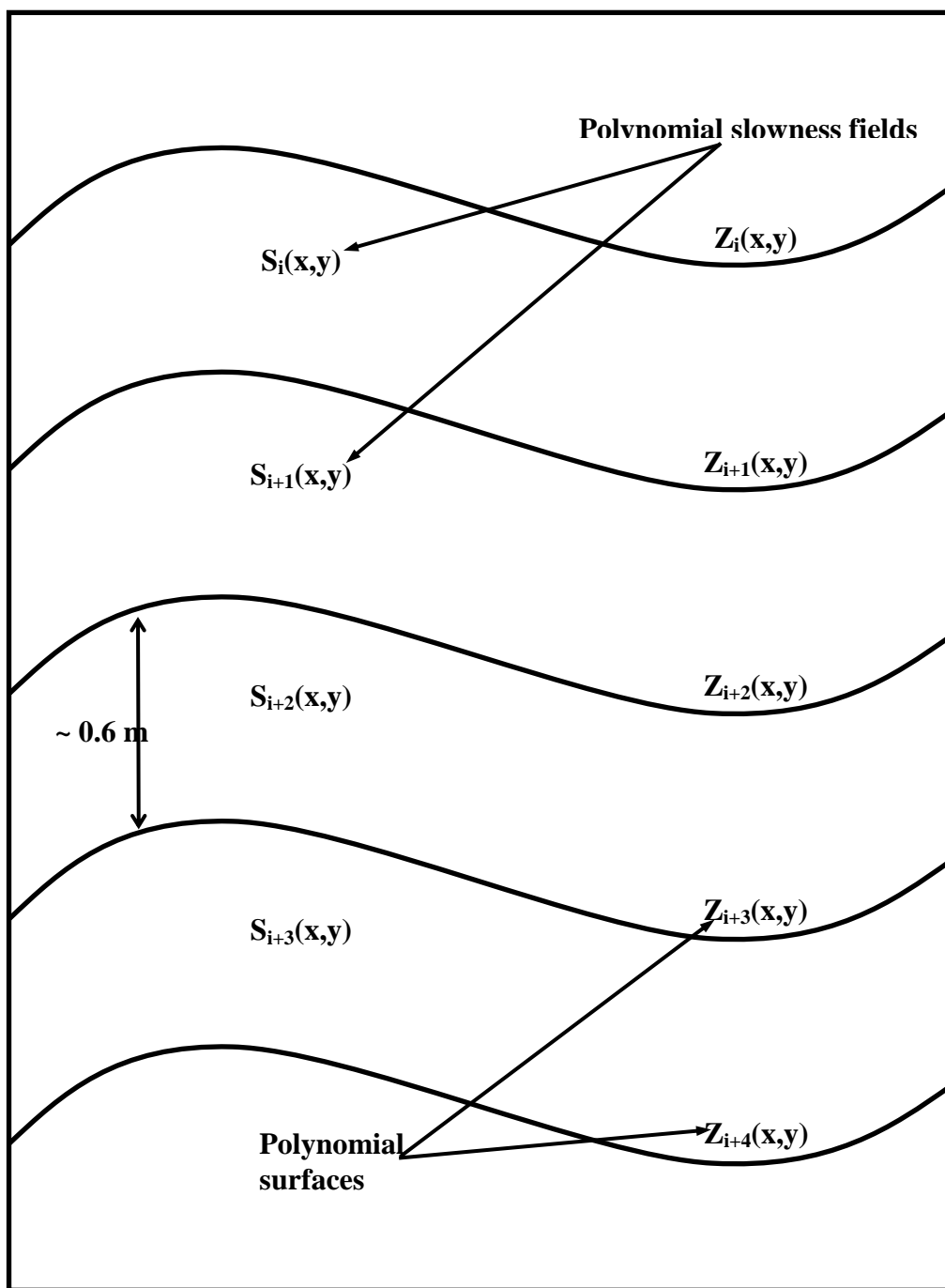


Figure 4. Schematic of common earth model geometry (vertical slice through 3-D model)

The 2-D Chebyshev polynomials are a limited tensor product of 1-D Chebyshev polynomials, keeping only terms of up to 3rd order. Equation 1 shows the form of the polynomials.

$$\begin{aligned}
 F(x, y) = & \\
 & + C_0 \\
 & + C_1x + C_2y \\
 & + C_3xy + C_4(2x^2 - 1) + C_5(2y^2 - 1) \\
 & + C_6(2x^2 - 1)y + C_7(2y^2 - 1)x + C_8(4x^3 - 3x) + C_9(4y^3 - 3y)
 \end{aligned}
 \tag{Eq. 1}$$

The coefficients C_0 through C_9 weight the contributions of the orders of the polynomial. There is a constant term (C_0), two first-order terms (C_1 and C_2), three second-order terms (C_3 through C_5) and four third-order terms (C_6 through C_9). By weighting the coefficients it is possible to fit surfaces of varying spatial smoothness. These ten coefficients provide essentially cubic variability in structure and velocities. While certainly insufficient to represent some scales of geologic heterogeneity, a large class of real world crosswell problems can be adequately treated with this representation.

The structural part of the model is constrained to be geologically realistic by fitting the surfaces to horizon picks from wireline log correlations in the wells. The coefficients for the Chebyshev polynomials are found by singular value decomposition of this data. Figure 5 shows a real example of different order surfaces fit to horizon picks from a series of five deviated wells in Chevron's Buena Vista Hills field in Kern County, California (Langan, et al., 1998). The horizon picks from wireline logs are shown as colored cubes in Figure 5a. Zero-order surfaces are horizontal, and would be used only in the absence of *a priori* geologic or well-log information about structure. First-order surfaces are constant dip and plunge planes, appropriate when there is limited well-log information available (Figure 5b). Second- and third-order surfaces are appropriate when there exists *a priori* information from a number of neighboring wells in areas of structural complexity, as in Figures 5c and 5d.

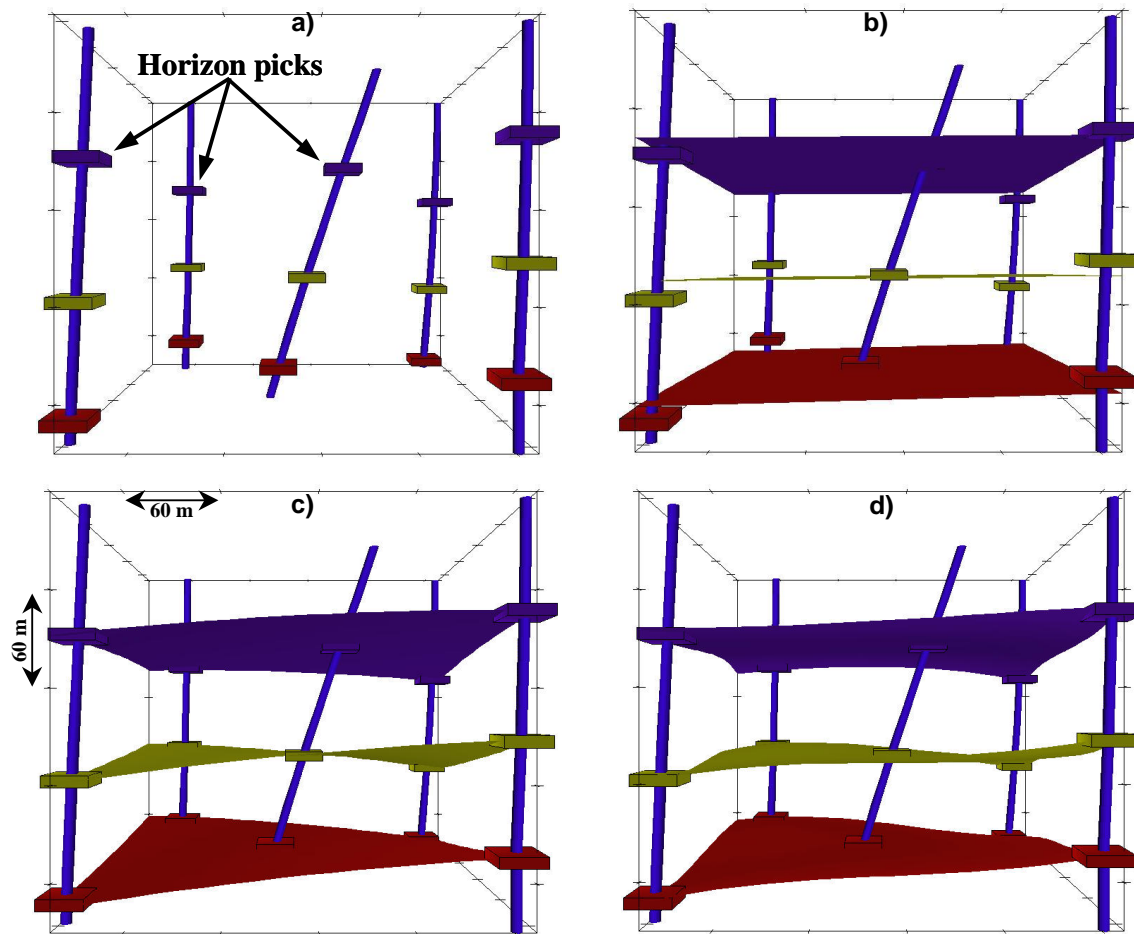


Figure 5. Chebyshev polynomial surfaces fit to horizon picks in deviated wells:

- a) horizon picks**
- b) first-order surfaces fit to horizon picks**
- c) second-order surfaces fit to horizon picks**
- d) third-order surfaces fit to horizon picks.**

The model used for tomography is obtained by interpolating the initial surfaces to a nominal vertical spacing of less than one meter. Figure 6 demonstrates an elevation view of a series of surfaces in the vicinity of a pair of deviated wells that for clarity have been interpolated to the coarser nominal spacing of 7.5 m. After this initial interpolation of the *a priori* “horizon pick” surfaces, the structural part of the model remains unchanged throughout the travelt ime inversion procedure; only the velocities in the layers between the structural surfaces can change.

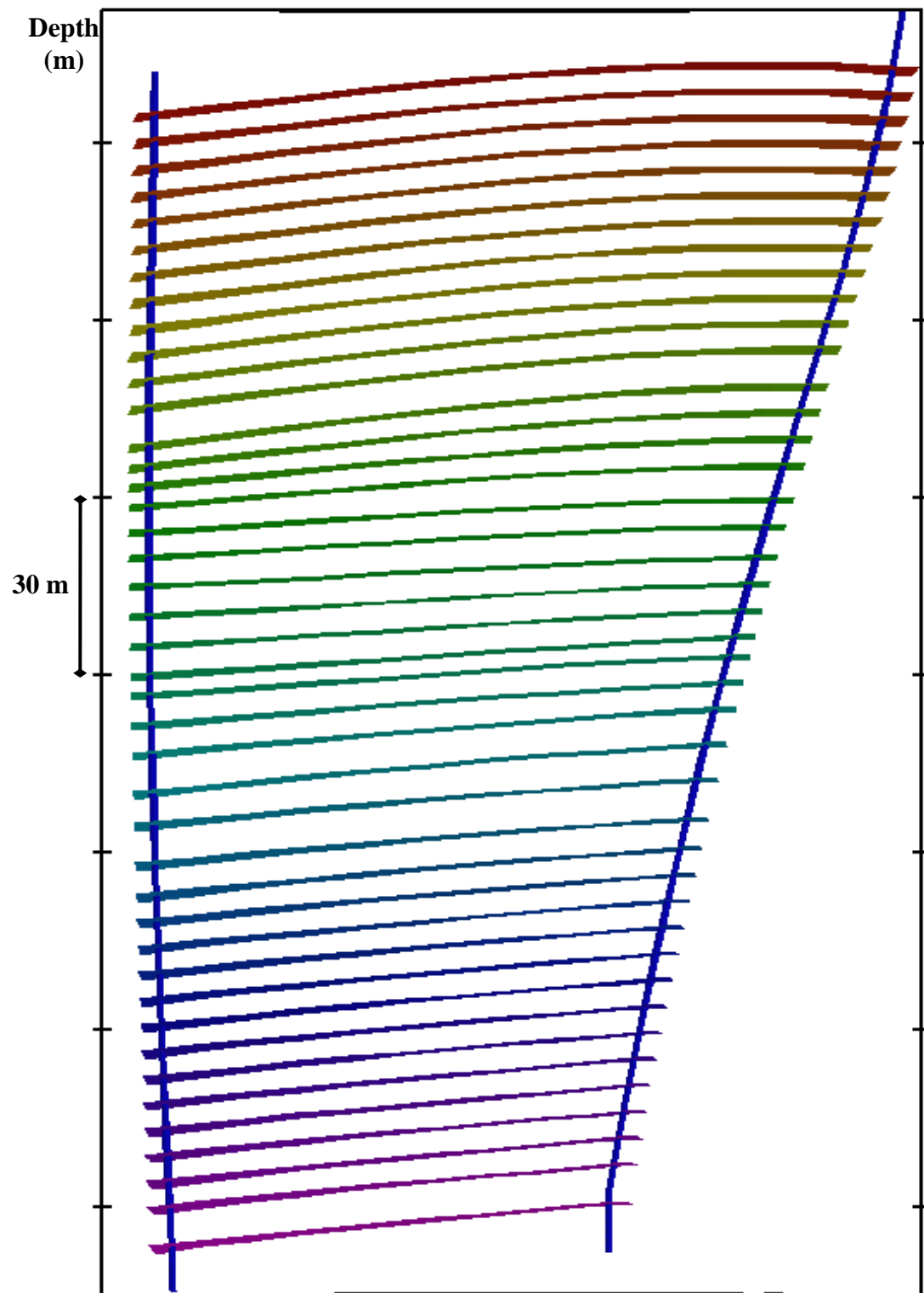


Figure 6. Elevation view of surfaces in the vicinity of a pair of deviated wells interpolated to nominal spacing of 7.5 m.

Traveltime Calculation and Ray tracing

The type of ray tracing used in crosswell tomography has been studied extensively. Iterative solutions to the tomographic problem require ray tracing for accuracy, particularly when strong velocity inhomogeneities are present. Although the “shooting method”—propagation of rays by successive application of Snell’s law at interfaces or cell boundaries—has widespread use, high wavenumber fluctuations in velocity can cause it to fail. In addition, the computational overhead to obtain accurate raypaths through high vertical resolution models is large even in 2-D, and for 3-D becomes prohibitively expensive.

The “bending method”, in contrast, is a fast two-point perturbative approach that relies on Fermat’s principle of least time. The two point method can provide solutions where a propagator method can fail. Another clear advantage of the bending method is that it can be expected to operate much faster than the shooting method for 3-D problems. For these reasons we employ the bending method.

The use of Chebyshev polynomials for the model parameterization introduces algorithmic advantages for the ray tracing because we can analytically calculate traveltime and derivatives. Furthermore, the individual polynomials are laterally continuously differentiable throughout the model, and the small number of parameters required improves the stability and robustness of both the forward problem (ray tracing) and the inverse problem (velocity inversion).

There are two assumptions involved in the forward modeling and traveltime calculation:

Slowness within a layer is a function of x and y , but invariant of z .

Raypaths are straight lines between layer boundaries.

These assumptions hold to first order because layer spacing is chosen small compared to wavelength for most crosswell data. The traveltime integral for a single layer is given by Equation 2, and the solution can be simply calculated in parametric form. The corresponding geometry is shown in Figure 7.

$$t = \int_A^B S(x, y) dl \quad \text{Eq. 2}$$

where t is the traveltime, $S(x,y)$ is the polynomial slowness within the layer, A and B are the intersection locations of the raypath with the surfaces that bound the layer, and dl is a differential element of length along the path from A to B . The total traveltime for a ray intersecting many layers is given by the sum over the individual segments.

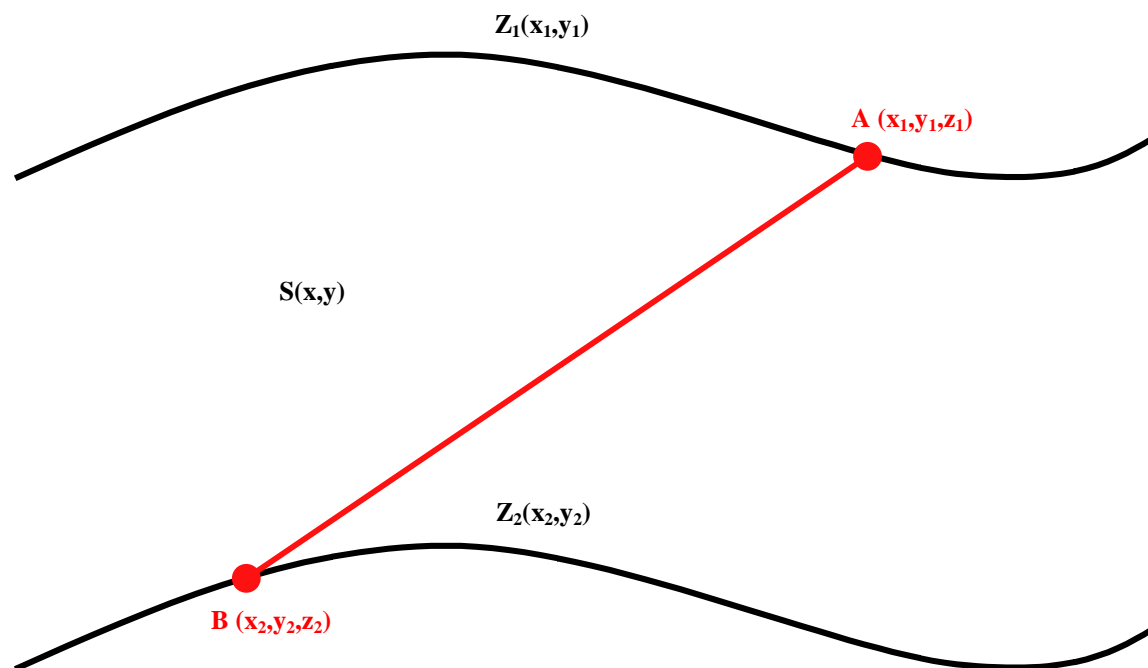


Figure 7. Schematic of geometry for traveltime calculation within a layer.

To ray trace with the bending method, we start with the straight ray connecting source and receiver, and minimize traveltime by iteratively finding perturbations to the raypath. Due to the vertical stratification of the model, z on the surfaces is a function of x and y , and the dimensionality of the problem is reduced to solving only for the updates to x and y at the intersections of the raypath with the surfaces.

Using Newton's method to solve the nonlinear ray tracing problem yields an elegant structure for the successive linearized problems. According to Fermat's principle, the ray with the minimum traveltime arrives first. Thus to compute first arrivals, the objective function that we minimize is traveltime, and derivatives of this functional with respect to the intersection locations can be determined in closed form. These partials only involve terms from adjacent layers, and the Hessian matrix of second derivatives is therefore band-diagonal and symmetric with nonzero elements in only three super-diagonals. The linear systems are quickly solved using matrix decomposition or factorization.

VSP-CDP Mapping—Algorithm Description

The VSP-CDP mapping for offset-VSP data is briefly described in this section.

The idea behind the VSP-CDP mapping is illustrated in Figure 8. Given a source-receiver pair, a trajectory can be defined that links all the possible reflection points for reflections recorded in this trace. For a horizontal reflector at a depth z_a , the corresponding reflection point is A, for a horizontal reflector at a depth z_b , the corresponding reflection point is B, for a horizontal reflector at a depth z_c , the corresponding reflection point is C and so on. The mapping trajectory is defined by linking the possible reflection points for all depths. Once the trajectory is defined, every sample of this trace is mapped on the reflection point for which the total reflection traveltime is equal to the time this sample is recorded. This procedure is repeated for all traces in the gather.

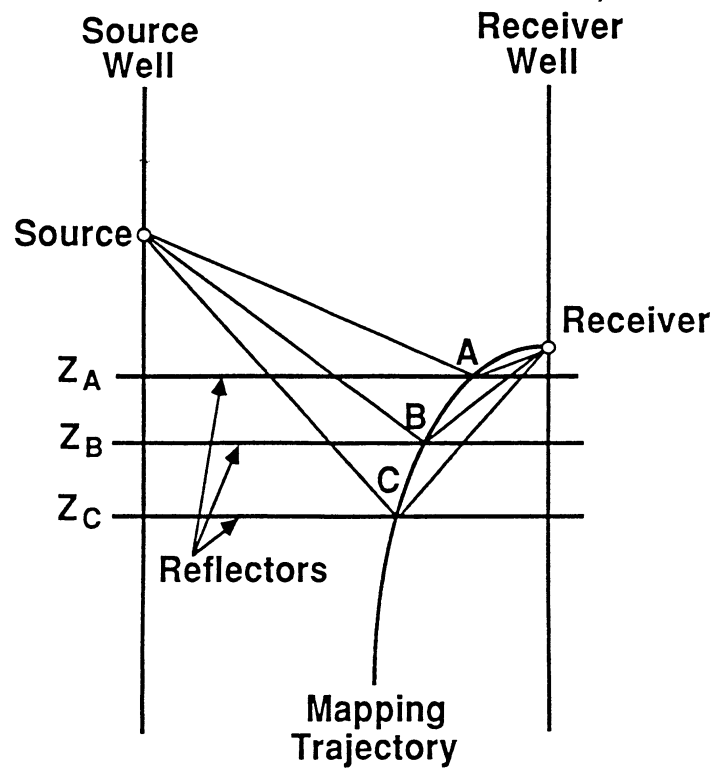
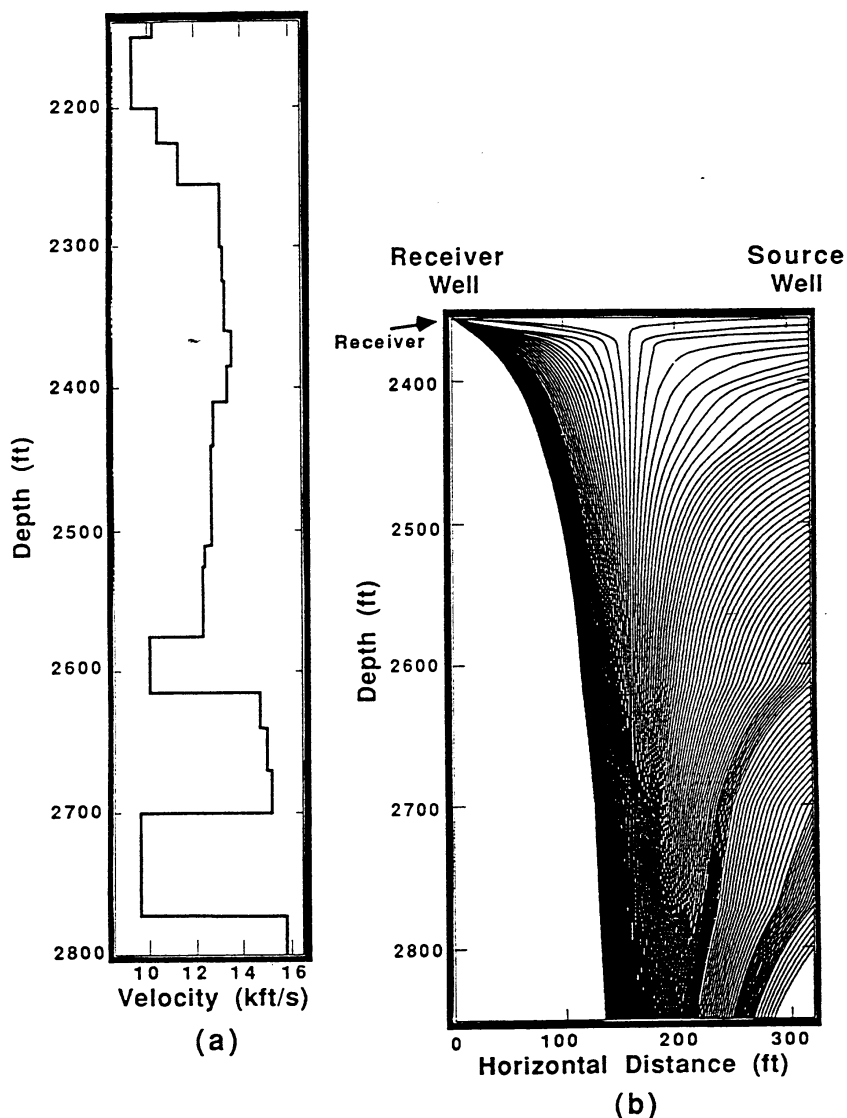


Figure 8. Construction of mapping trajectories.

For a constant velocity, the mapping trajectories and corresponding traveltimes can be calculated analytically. For more general velocity backgrounds, they can be calculated by ray tracing. A 1-D velocity model is shown in Figure 9a. Mapping trajectories, calculated by ray tracing through this model, are shown in Figure 9b. These are trajectories for a common receiver gather. Every trajectory corresponds to a source.



**Figure 9. (a) 1-D velocity model
(b) mapping trajectories for a common receiver gather,
calculated by ray tracing through the 1-D model**

Trajectories that start from the source well (on the right-hand part of the plot) correspond to sources located at depths larger than the receiver depth. The group of trajectories that start from the receiver location (on the left-hand part of the plot) corresponds to sources located at depths smaller than the receiver depth. Although the algorithm was conceptually described as the operation of spreading traces along the reflection point trajectories, the actual implementation used is different. It is based on the generation of maps, attributing each point in the image the following quantities:

- Depth of the receiver (source for a common receiver gather) at which a specular reflection for a horizontal reflector passing through this point will be recorded.
- Reflection traveltimes
- Reflection moveout. This is the dip of the reflection event in the data.

Characteristics of VSP-CDP Mapping

Dipping reflectors

- Mispositioning due to dip scales with the interwell distance and does not depend on velocity
- Independent of the true dip and true azimuth and the dip and azimuth assumed by the imaging algorithm, reflection points at the wells will be mapped to their correct location
- Lateral mispositioning is greater than vertical mispositioning
- When imaged with a horizontal reflector algorithm, in-plane dipping reflectors are pulled up between wells
- When imaged with a horizontal reflector algorithm, out-of-plane dipping reflectors can be either pulled up or pulled down
- Lateral mispositioning is not very sensitive to the azimuth of the reflector. This suggests that imaging algorithms designed for in-plane dipping reflectors would position reflection points to an approximately correct horizontal location
- Reflector pull ups and lateral mispositioning tend to increase with angle of incidence
- For wider angles of incidence, the true reflection points for out-of-plane dipping reflectors are closer to the interwell plane.

Velocity

- Mispositionings due to velocity inaccuracies depend on the percentage of velocity error, not on its absolute value
- Both vertical and lateral mispositionings scale with the interwell distance
- Vertical mispositioning is smallest for intermediate angles and increases for small or large angles. It does not depend on the horizontal location of the reflection point
- Lateral mispositioning is largest for reflection points close to the wells and decreases to zero for reflection points located halfway between wells
- As the ratio of interwell distance over wavelength increases, a more accurate velocity is needed to stack crosswell reflections

Stretch

- Both vertical and horizontal stretches increase with angles of incidence
- Vertical stretch is independent of the location of the reflection point. Lateral stretch is largest closest to the wells and decreases as we move towards the middle.
- Loss of resolution due to stretch depends on the wavelength and is independent of the interwell distance

Lateral Resolution

- The size of the Fresnel zone (both in-plane and out-of-plane) scales with the interwell distance
- The in-plane size of the Fresnel zone increases with increasing incidence angle
- The out-of-plane size of the Fresnel zone decreases with increasing incidence angle.

Information from this section was derived from Lazaratos S., Crosswell Seismic Imaging, Ph.D. Dissertation, Stanford University, January 1993.

Migration

Migration of crosswell data has similarities to surface seismic migration but has unique considerations for the crosswell geometry. We choose a post-CDP mapping approach (over a pre-map migration) because of several advantages:

- Greater robustness where the initial velocity model may be inaccurate
- Operational efficiency
- Imaging in depth
- Ability to attenuate coherent noise modes prior to migration with post-map stacking over subsets of the data.

Imaging algorithms for crosswell reflection data have developed on the basis of either of two theories, wave theory or ray theory. Prestack migration based on wave theory optimally collapses diffraction energy and shrinks the Fresnel zone. However, like other prestack migration techniques, its performance could be degraded with low signal-to-noise ratio (SNR) data since coherent and incoherent noise are smeared along the imaging ellipse. Crosswell data typically have large levels of coherent noise in the form of mode-conversions, guided waves, multiples, and tube waves. Even after applying wavefield separation filtering, the SNR may not be adequate for performing prestack migration. Also, like other migration-type algorithms, the distortion occurs at the edge of the image due to the limitation of the migration aperture.

When adapted for the crosswell geometry, VSP-CDP mapping is another technique that is used to image crosswell reflections. The VSP-CDP mapping transforms the crosswell data from (source depth, receiver depth, traveltimes) to (common reflection point, incidence angle, depth). VSP-CDP mapping is a ray-theoretical migration which correctly positions specular reflections in the interwell region. In VSP-CDP mapping, every sample of each trace is mapped on the possible reflection point for which the total reflection travel time is equal to the time this sample is recorded. Since VSP-CDP mapping is a point-to-point transformation, it can be considered as a zero aperture depth migration and it does not smear noise like prestack migration techniques. Therefore, it is a more robust method for imaging crosswell reflections. However, because of the large vertical stretch in the wavelet at wide incidence angles after VSP-CDP mapping and source radiation pattern, we use only data corresponding to incidence angles of limited range for imaging. Also, it can only handle a single dip at one time, and it does not collapse diffractions. So, a diffraction-collapsing step is still needed to improve the lateral resolution of the mapped image. If we can improve the lateral resolution of the mapped data by applying a migration-type algorithm after mapping *and* limited stacking, we can achieve the best imaging method, one which is robust for low SNR crosswell reflection data yet also collapses diffractions.

To perform post-map migration, we sum the seismic amplitudes along the moveout curve of a diffractor under the assumption that reflectors in the subsurface can be visualized as being made up of such many point diffractors. Since the obliquity term of the wavelet after wavefield separation and VSP-CDP mapping may not be well approximated by the standard Kirchhoff integral, we don't consider the change in the amplitude due to the wave propagation. Also, we reduce the edge effects near the wells, one of the problems with crosswell premap migration techniques, by controlling the post-map migration aperture.

Control of Migration Aperture

In imaging seismic reflection data with migration, distortion occurs at the edge of the image due to the limitation of the migration aperture. To suppress the edge effects in surface seismic migration, seismic data are usually collected over a wider region than the region of interest. However, in crosswell reflection seismic, the area where the data are obtained is limited by two wells, and the image will be distorted near

the wells. Even when we apply post-map migration to VSP-CDP mapping with full migration aperture, the edge effect occurs near the wells and the migrated image is distorted. To reduce these edge effects, we control the post-map migration aperture using a measure of the derivative of the diffraction curve. The aperture width is the greatest at the center and becomes smaller as a diffractor moves closer to the wells.

Angle Transform

The VSP-CDP mapped data set is a 3-D data cube as shown in Figure 10.

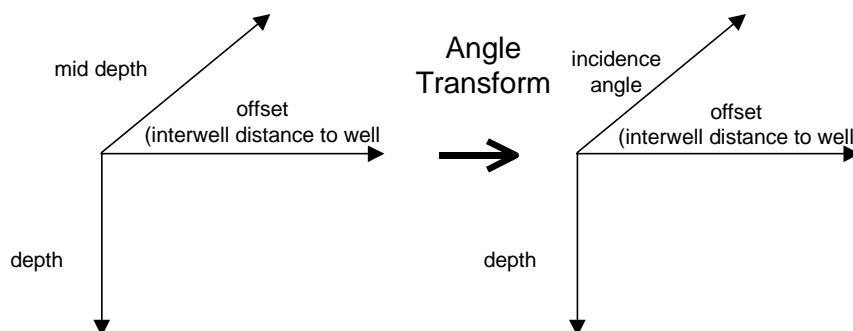


Figure 10. VSP-CDP mapped data with angle transform.

Because of the wide range of incidence angles present on a crosswell data set and because of the wavelet and reflection character change with incidence angle, another natural domain transforms the data with the angle transform into the data cube as shown above. We call gathers from a single offset with angle as the changing variable, AVA (amplitude versus angle) gathers.

The transform typically used assumes straight ray paths and potentially planar dipping reflectors. The straight ray assumption makes the transformation smooth and well ordered. Ray tracing of models with significant velocity contrasts makes a “true” incidence angle transform potentially disordered. Therefore, the straight ray assumption is typically used.

AVA ANALYSIS

The amplitude versus angle gathers also provide opportunities for angle selection, noise rejection and velocity analysis. The synthetic AVA gather in Figure 11 shows wavelet changes and moveout stretch as a function of incidence angle. The synthetic seismogram accounts for both non-vertical incidence effects through complete evaluation of Snell's law at each interface and for the wavelet stretch that occurs as a function of incidence angle in VSP-CDP imaging.

Angle selection is used to select angles that maintain adequate SNR while best approximating the vertical incidence (0°) response. Angle muting can also be used to remove angle ranges where SNR is poor.

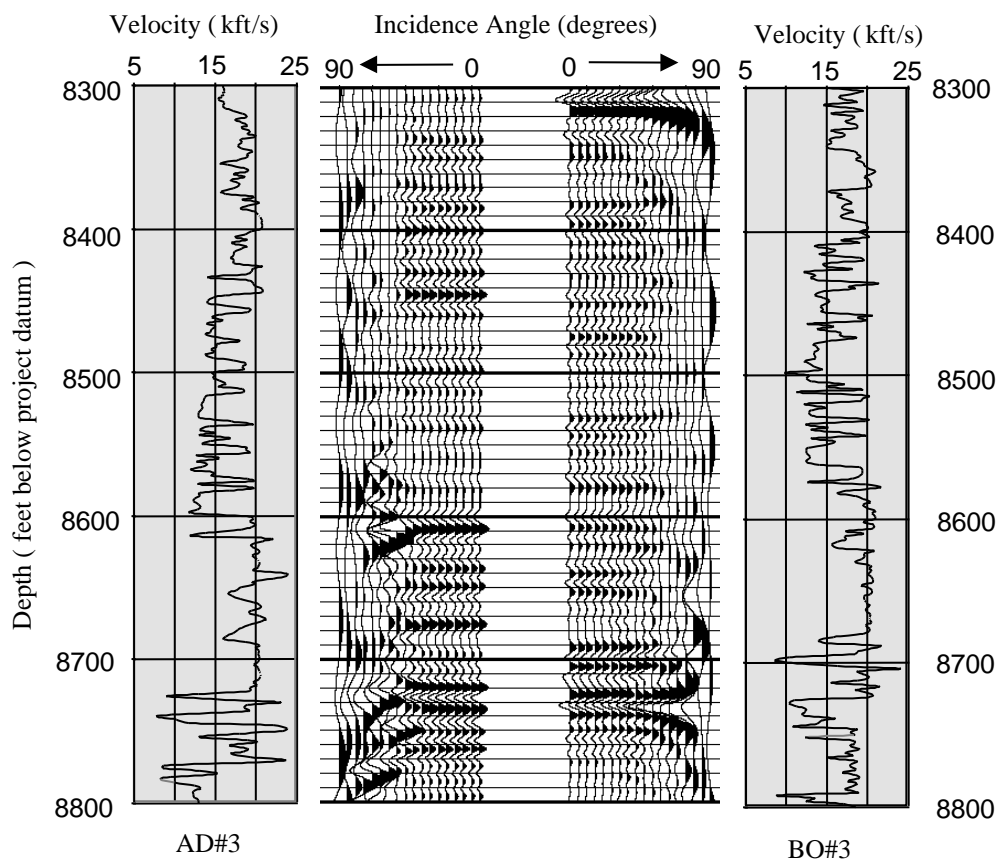


Figure 11. Non-vertical incidence synthetic seismograms for two well logs.

Reflection events should be flat in AVA gathers. Small velocity errors may result in small dips for events in AVA gathers. Events with large dips from the horizontal are sometimes filtered in AVA gathers.

velocity analysis

Since events should be flat in AVA gathers, we can perform velocity analyses and updating in AVA gathers. Correlation-based shifts are calculated for each trace in the AVA gather. The shifts are constrained to small vertical shifts and smooth lateral variations to provide a model-consistent set of shifts.

Stack

Based on the selected angle ranges and velocity/residuals updates, a stack of the reflection data is produced resulting in a 2-D offset versus depth image. Brute stacks over a range of wide angles with no velocity analysis are used for preliminary QC. Stacks over a limited angle range (e.g. $55^{\circ} - 60^{\circ}$, $60^{\circ} - 65^{\circ}$, etc) are often used to assist in angle selection.

APPENDIX C – ANISOTROPY PROCESSING

Summary

Seismic velocity anisotropy has been observed in a variety of geologic settings and is being recognized as an important issue in surface seismic data processing. Strong evidence of TI (“transversely isotropic”) velocity anisotropy has been observed in many crosswell data volumes especially in deep, well consolidated shale formations. The crosswell seismic acquisition geometry produces data along a variety of angles from the bedding plane and therefore provides a unique measurement for characterizing TI anisotropy. The ability to estimate TI anisotropy from crosswell seismic data has several benefits:

- Formation characterization. TI anisotropy can be an indicator of shaliness and of the presence of parallel fractures.
- Crosswell imaging enhancement. A more exact description of the velocity field provides opportunity to enhance both the crosswell velocity image and reflection section.
- Quantification of TI anisotropy for surface seismic processing. TI anisotropy is often thought to be a factor in surface seismic imaging. Techniques exist to image surface seismic data where TI anisotropy is present. Direct measurements of the velocity anisotropy reduce the need to iteratively image the data with a variety of anisotropy assumptions.

Schlumberger DeepLook Crosswell Seismic has developed a crosswell seismic processing approach to detect and quantify TI anisotropy and to apply the estimates of anisotropy in crosswell imaging.

PROCESSING APPROACH

A sequential approach is taken in incorporating TI anisotropy in crosswell seismic processing. The approach has the objective of measuring meaningful TI anisotropy that is characteristic of the formations in the earth, rather than using an anisotropic “tweak” factor to make up for unexplained factors in the seismic processing. The processing steps are:

- Detection of apparent anisotropy
- Confirmation of formation anisotropy
- Estimation of formation anisotropy
- Application of anisotropy parameters in ray tracing for imaging.

DETECTION OF ANISOTROPY

To confirm the presence of anisotropy, we perform isotropic tomography over a suite of narrow ranges of incidence angle. The fully 3-D tomographic algorithm is used for this to minimize any geometry effects due to well deviations and structure, which could affect the traveltimes. An example of a limited angle panel for a reservoir with TI anisotropy is shown in Figure 1.

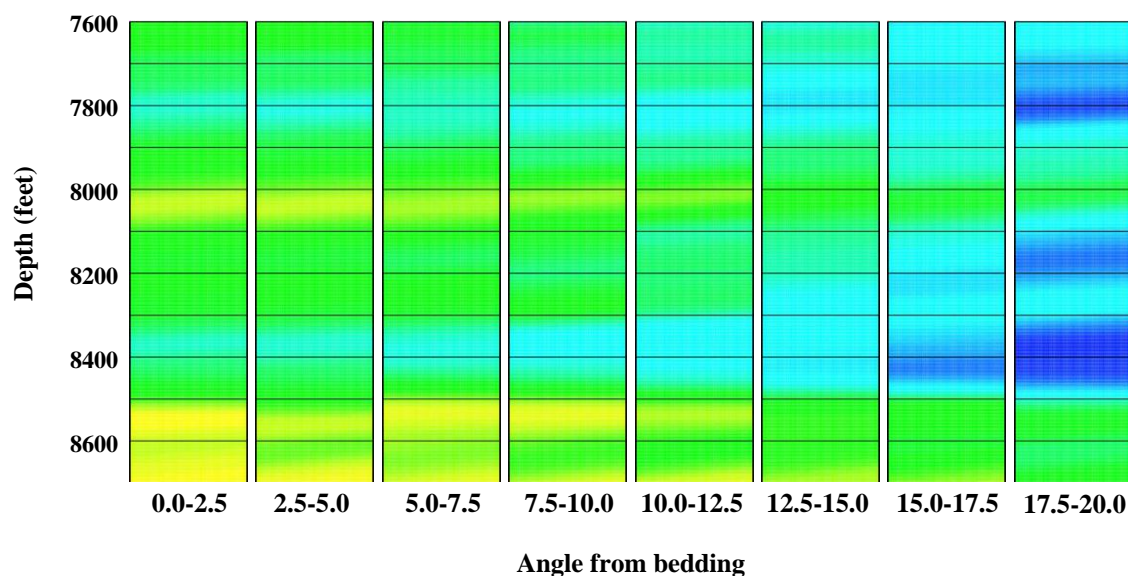


Figure 1: Narrow angle tomography panels showing differences in velocity with angle from bedding before anisotropic corrections. Velocities range from 3.85 km/s (blue) to 4.55 km/s (red).

Confirmation of Anisotropy

For isotropic media with no systematic errors in the data acquisition or traveltime estimation, each limited angle tomogram should have similar velocity values. Formation anisotropy or errors in survey geometry can produce changes in measured velocity in the tomograms as a function of incidence angle. The positions of source and receiver are measured using wellbore deviation survey data and the measured wireline depth from crosswell data logging. The vertical accuracy in position is usually dominated by errors in wireline depth. Precision wireline depth control maintains such errors at values of 1 foot or less. Horizontal accuracy in position is dominated by errors in the deviation survey. Precision rate gyroscopic deviation surveys at most depths provide accuracies of 1% or less. Other forms of deviation survey data such as accelerometer based measurements, multishot surveys or single shot surveys, can produce greater errors. Larger relative horizontal positioning errors can also occur when wells are very closely spaced (less than 100 feet apart). When larger horizontal positioning errors are present (relative to the accurate vertical positioning), vertical and horizontal velocities obtained by tomography will be different. This difference can mimic TI anisotropy (horizontal velocity less than vertical velocity) or can be of the opposite sense. Apparent anisotropy induced by positioning errors does not vary with formations and typically varies slowly with depth since deviation survey errors are typically a “drift”. If the apparent anisotropy detected in the limited angle panels has the characteristics of positioning-induced anisotropy,

survey geometries are corrected prior to further processing. The correction may be made by one of several methods:

- Correcting inaccurately entered information
- Acquiring more accurate wellbore surveys
- Applying well positioning correction algorithms based on reduction of apparent anisotropy

Remaining apparent anisotropy in the limited angle tomogram panels that correlates with formation changes is strong evidence of TI (transversely isotropic) anisotropy.

Estimation of Anisotropy

We solve directly in the traveltimes inversion for parameters that describe TI anisotropy. Our general approach to crosswell traveltimes tomographic inversion is to solve for velocities in thin layers, allowing for lower lateral than vertical variability in velocity. Typical layer thickness is 2 to 4 feet. When solving for parameters describing TI anisotropy, we estimate the parameters in each layer of the velocity model as shown in Figure 2.

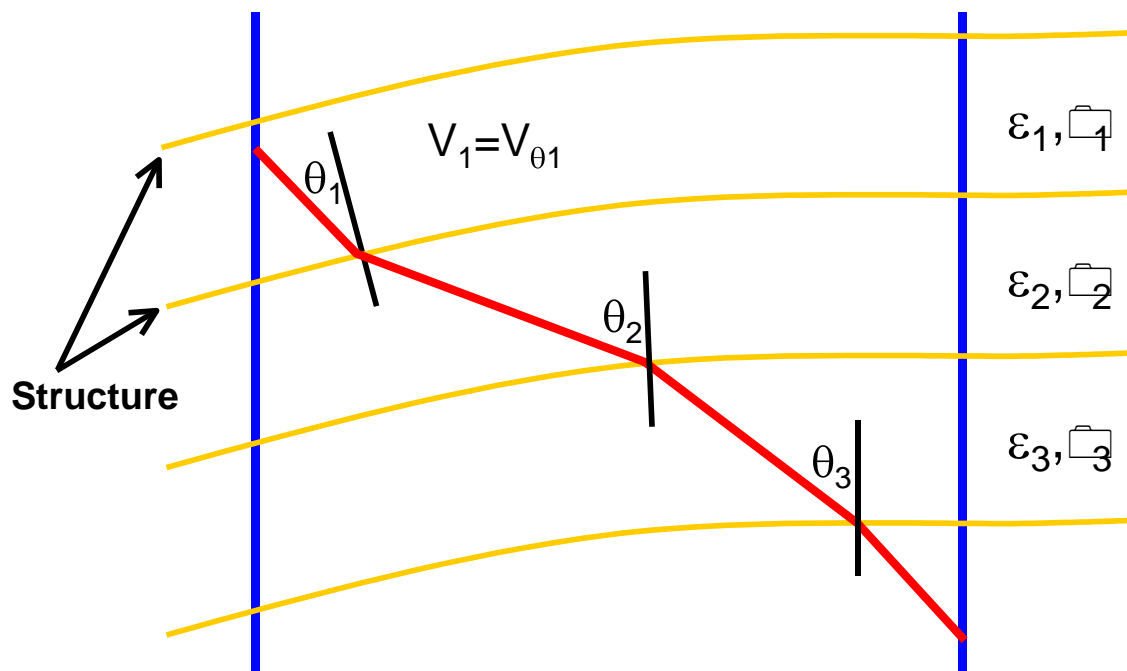


Figure 2: The layered earth model with anisotropy parameters describing each layer

Angle is defined relative to the bedding plane in each layer.

The inversion solves for anisotropy parameters from one of 2 descriptions of anisotropy:

- Elliptical anisotropy
- Akhalifah and Tsvankin parameterization

The anisotropic parameterization we use is derived from Thompson (1986) who established a simple two-parameter relation for the variation of velocity with respect to angle:

$$V_{\theta} = V_z \left[1 + \delta \sin^2 \theta \cos^2 \theta + \varepsilon \sin^4 \theta \right] \quad \text{Eq. 1}$$

where V_{θ} is the velocity for seismic energy traveling at a particular angle θ measured from the vertical, V_z is the velocity for energy traveling vertically, and the parameters δ and ε are directly related to elastic moduli and calibrate the anisotropy. For the crosswell geometry, horizontal velocities can generally be well resolved from small-offset tomography. The vertical velocities, however, are largely undetermined. We therefore reformulate equation (1) in terms of the crosswell zero-offset or horizontal velocity V_H . At the horizontal the term involving δ vanishes. We can then replace V_z by $V_H / \sqrt{1 + \varepsilon}$, where V_H is the crosswell zero-offset velocity. The clear difference from anisotropic treatments in surface reflection work is that we have "normalized" everything by the zero-offset crosswell velocity (horizontal velocity) rather than the zero-offset surface velocity (vertical velocity).

Akhalifah and Tsvankin (1995) introduced the parameter η , defined as $\eta = \left[\frac{\varepsilon - \delta}{1 + 2\delta} \right]$, which we use to reformulate Eq. 1 for the crosswell geometry.

$$S_{\theta} = S_H \left[1 + \varepsilon \cos^2 \theta + \eta \left[\cos^2 \theta - \cos^4 \theta \right] \right] \quad \text{Eq. 2}$$

$$\text{where } S_{\theta} = 1/V_{\theta}$$

$$\text{and } S_H = 1/V_H$$

The anisotropy parameters (η and ε) are used to make corrections along the raypaths in both the tomographic and the reflection ray tracing.

In the elliptical case $\delta = \varepsilon$; therefore, η becomes 0 and Eq. 2 becomes:

$$S_{\theta} = S_H \left[1 + \varepsilon \cos^2 \theta \right]$$

In the anisotropic inversion we solve for the velocity at a selected angle (often parallel to the bedding plane) and the anisotropy parameters. Figure 3 shows the data from Figure 1 following anisotropic inversion.

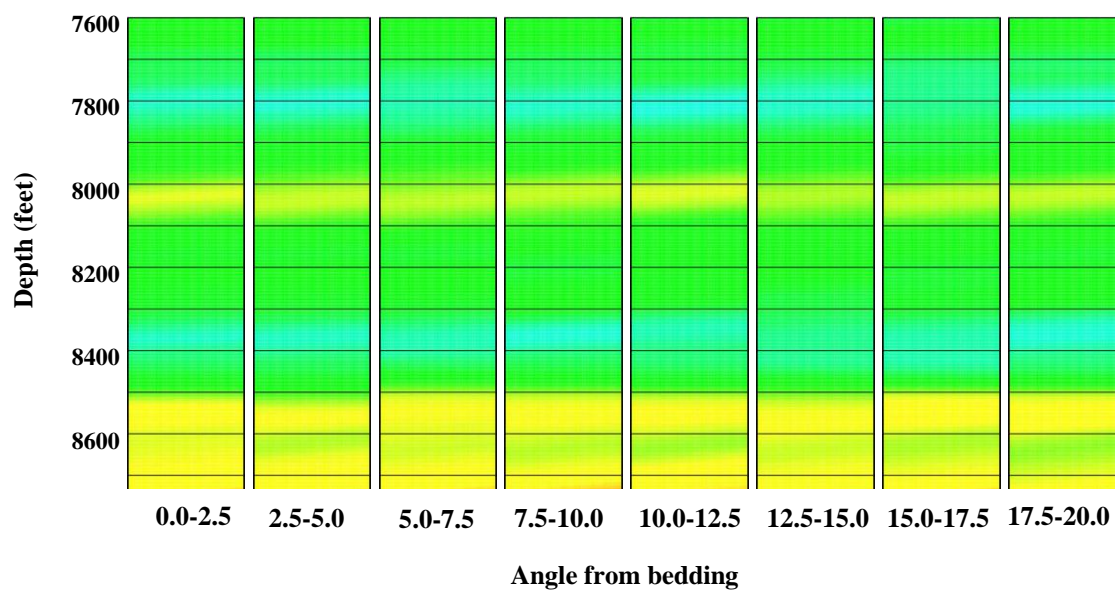


Figure 3: Narrow angle tomography panels showing differences in velocity with angle from bedding after anisotropic corrections.

Anisotropic Ray tracing

Once the parameters describing anisotropy in each layer of the model have been estimated, the ray tracing for reflection imaging is performed incorporating the description of anisotropic velocities from the inversion. If anisotropy is present and it is not corrected for, alignment of reflection events will be quite poor. Figure 4 shows the difference between the use of isotropic vs. anisotropic ray tracing in reflection processing. Notice that the reflections are flattened correctly for the anisotropic case.

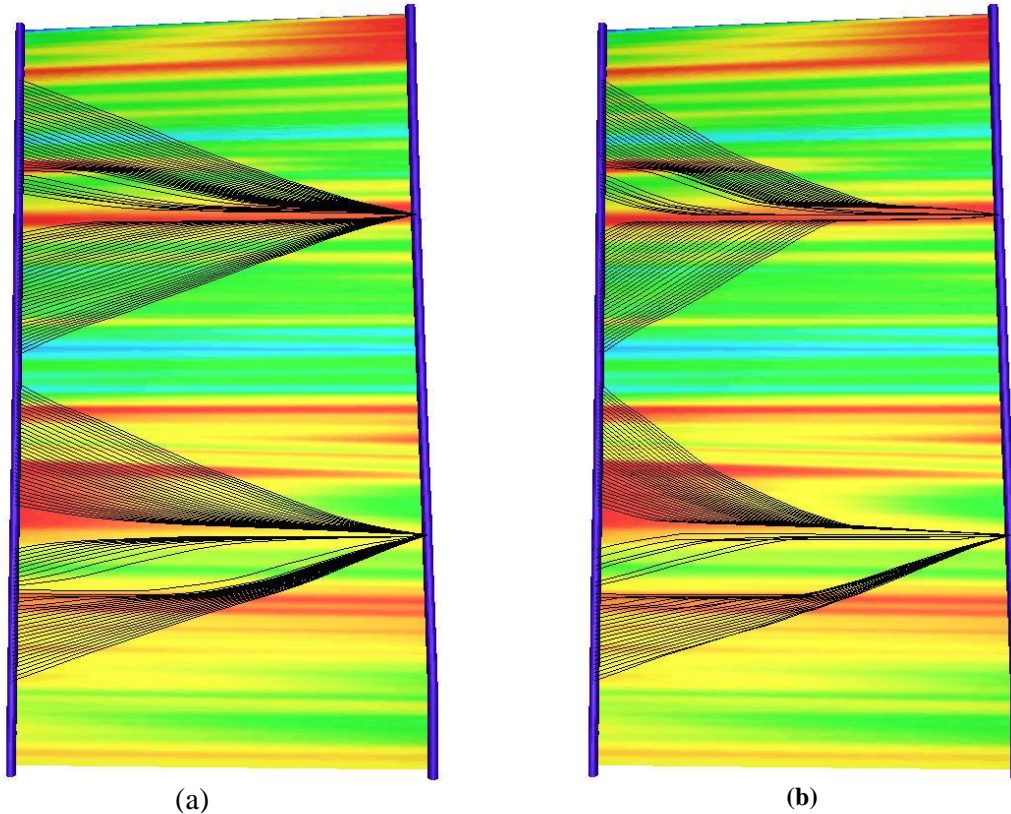


Figure 4: Angle gather showing reflections mapped using isotropic and anisotropic models. Corrections are made along raypaths for anisotropy.

We can see a larger amount of ray bending when anisotropy is present as shown in Figure 5. Therefore, the presence of large amounts of anisotropy cannot be neglected in the reflection imaging.

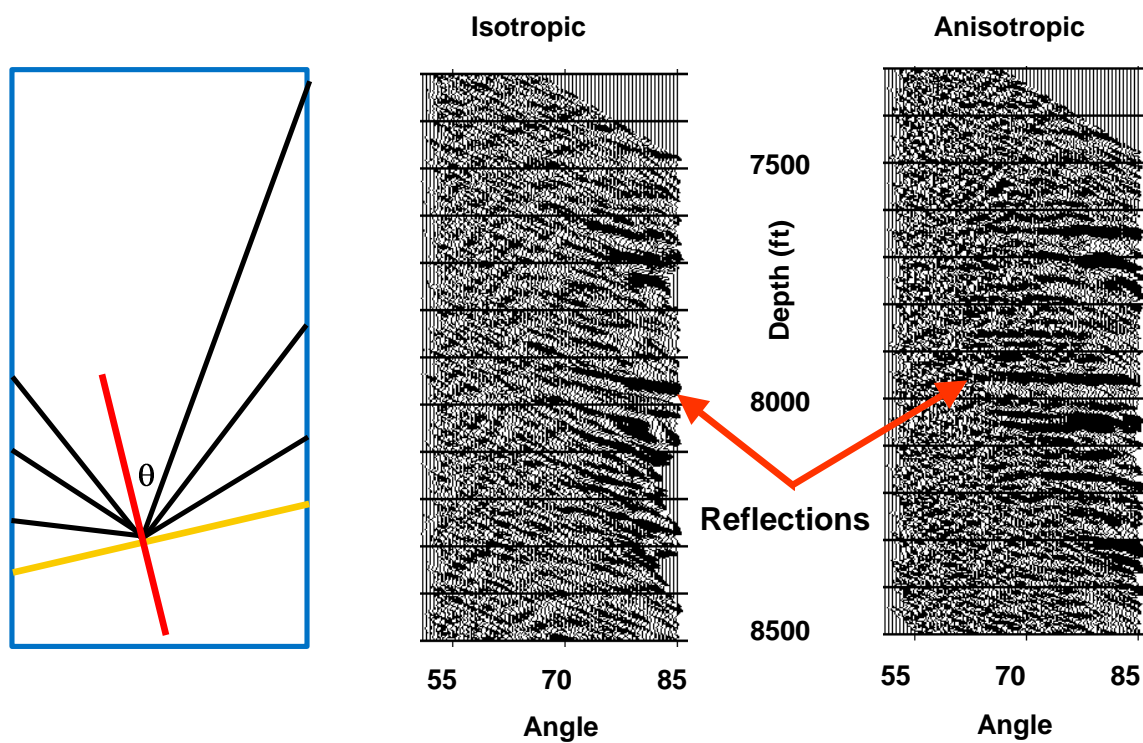
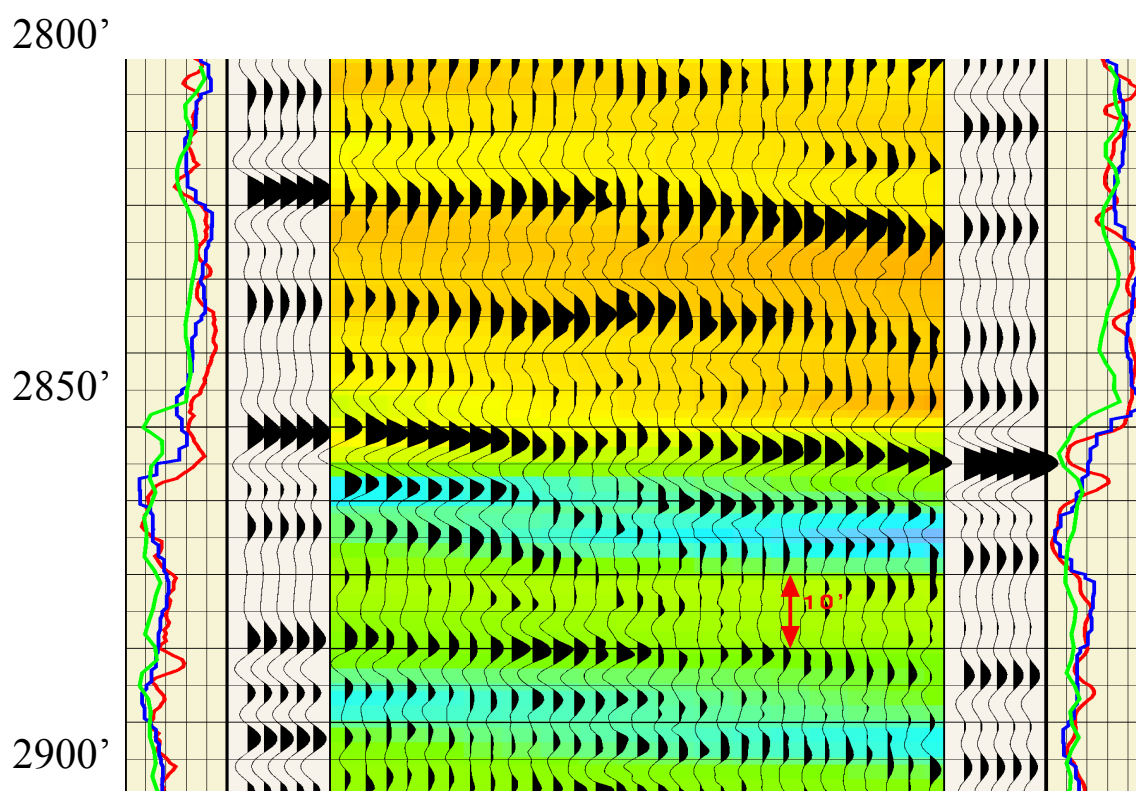


Figure 5: Raypaths through a model (a) without and (b) with anisotropy present in the model. Well paths are indicated in blue, colors between the wells indicate low velocities in blue and high velocities in red.

Log Scale INTERWELL IMAGING

Crosswell Methods and Glossary



CROSSWELL METHODS & GLOSSARY

Crosswell seismic imaging is a technique that produces images of structure and reservoir properties between wellbores at resolution 10 times that of typical surface seismic data. The crosswell technique has the unique ability to resolve reservoir-scale changes away from the wellbores, a key in unlocking perhaps the final oil and gas frontier: the interwell region.

Concept

In crosswell seismic imaging a seismic source is placed in a wellbore and receivers in a nearby wellbore as shown in Figure 1 to provide high resolution images and estimates of reservoir properties between the wells. The direct arrivals shown in Figure 1 are used in traveltimes tomography to estimate the formation velocity in the interwell region at the depths logged. The reflected rays, both downgoing and upgoing, are used to provide a seismic reflection image in the same region as the tomographic image, as well as above and below the depths logged. The advantages of crosswell imaging over surface seismic include the dramatic increase in available resolution in reflection imaging and the ability to directly measure a 2-D velocity field using tomography. The resolution of crosswell reflection imaging in carbonate reservoirs has been demonstrated to be 10 times or greater than that of surface seismic data, with vertical resolution of 5 to 10 feet.

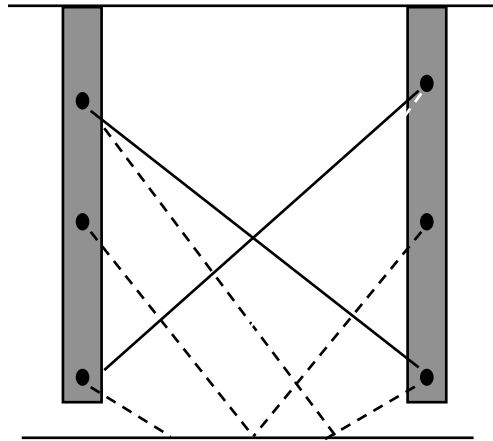
Two representations of the data are commonly used in crosswell seismics as shown in Figure 2:

- A velocity image describing the 2-D seismic velocity field between the wellbores
- The reflection image describing impedance boundaries in the earth between wellbores.

Traveltimes tomography typically produces velocity images with significantly lower resolution than the reflection image. Recent velocity analysis and inversion advances open the door to bridging the resolution gap between velocity images and reflection images.

Survey Planning

The driving factor in survey design is to obtain adequate coverage of the zone of interest. To ensure an adequate range of angular coverage for both tomography and reflection imaging, we use survey design and analysis tools to achieve required coverage at minimum cost. With these tools, a stacking chart shown in Figure 3 and the associated angular coverage and fold charts shown in Figure 4 are produced. Fine source and receiver level spacing for the survey is needed to acquire data that is not spatially aliased to allow good wavefield separation processing. For West Texas carbonate reservoirs, a



Direct arrivals (solid path) are used to estimate traveltimes and image the velocity field between wells.

Reflection energy (dotted path) images horizons between, above or below the zone logged.

Figure 1. Concept of crosswell seismic imaging.

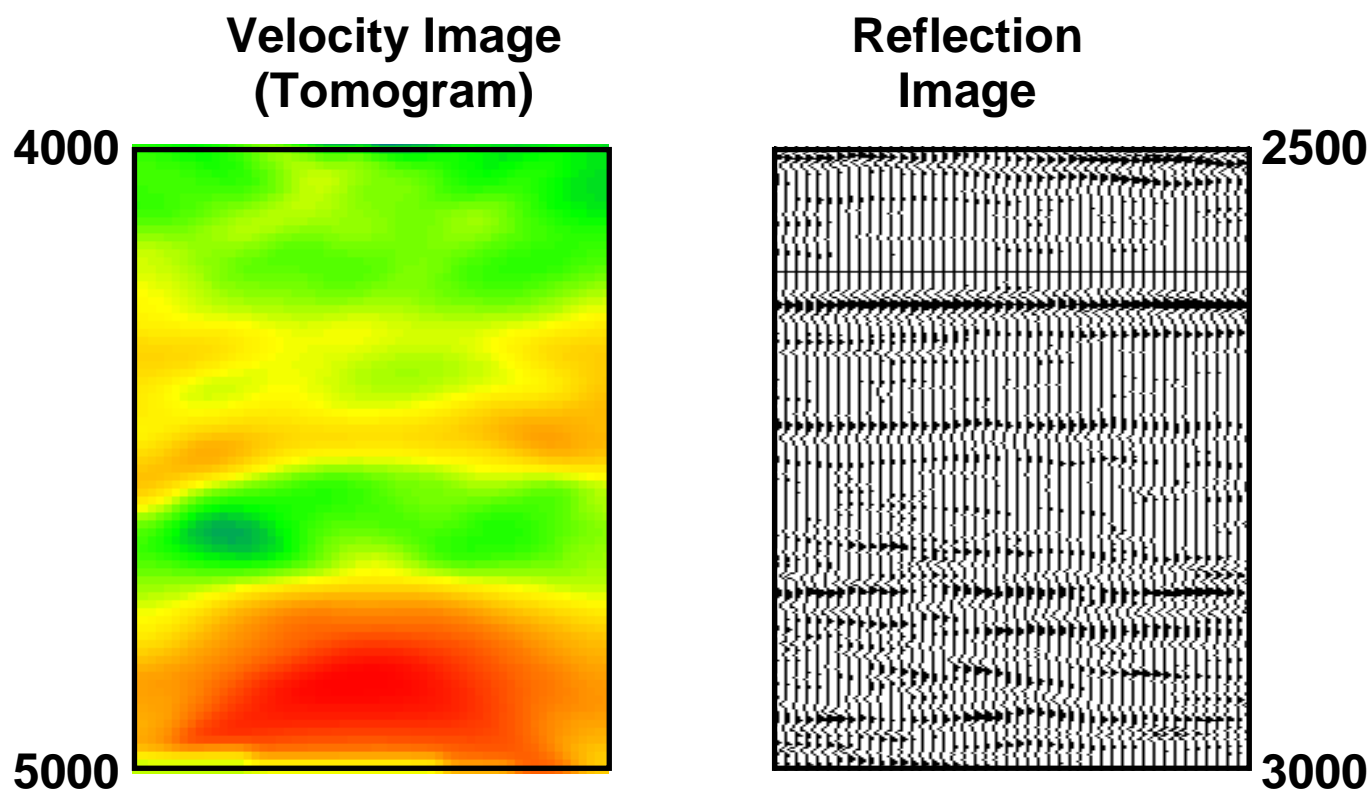


Figure 2. Two representations of crosswell data.

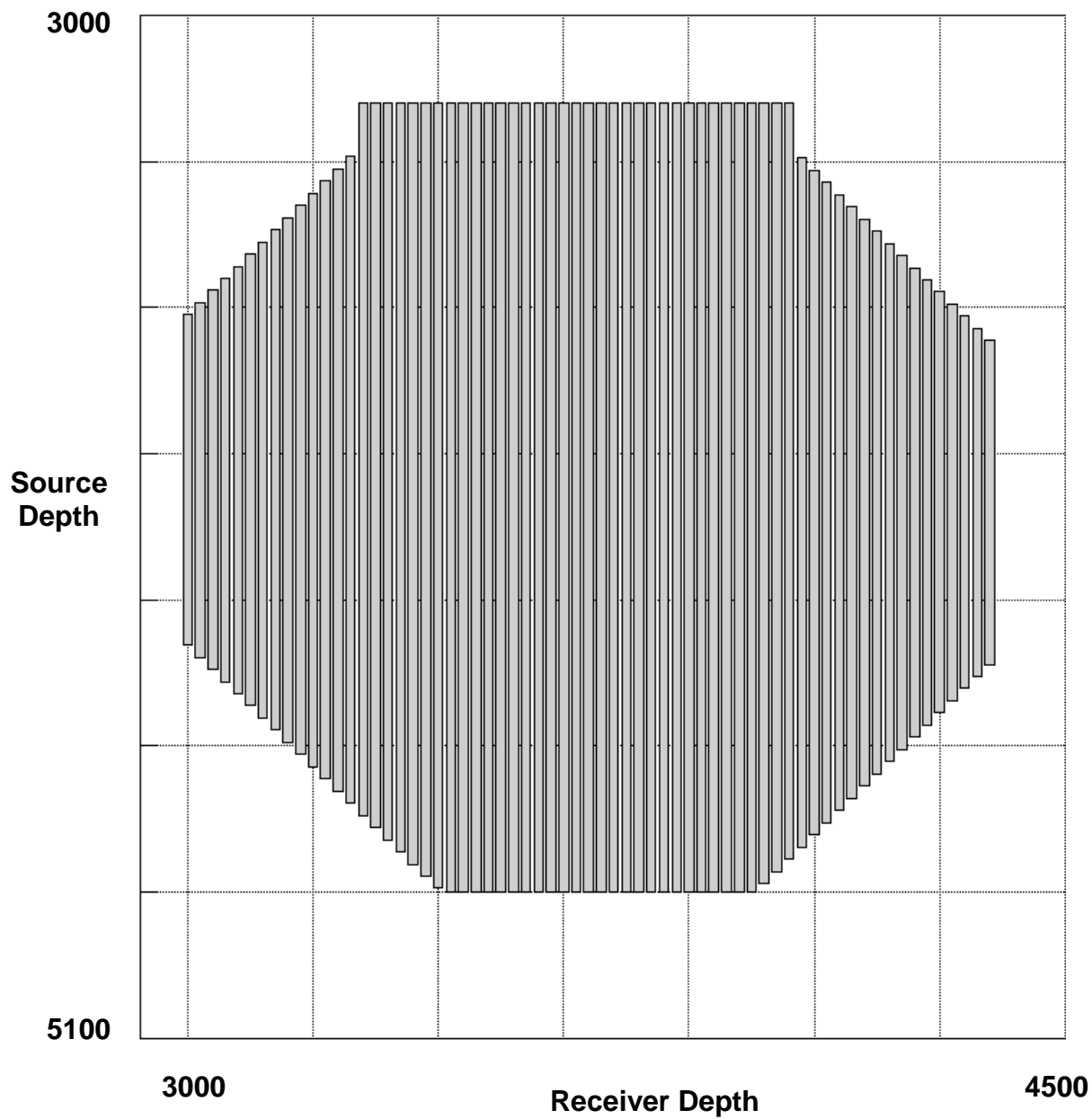


Figure 3. Crosswell shooting chart.

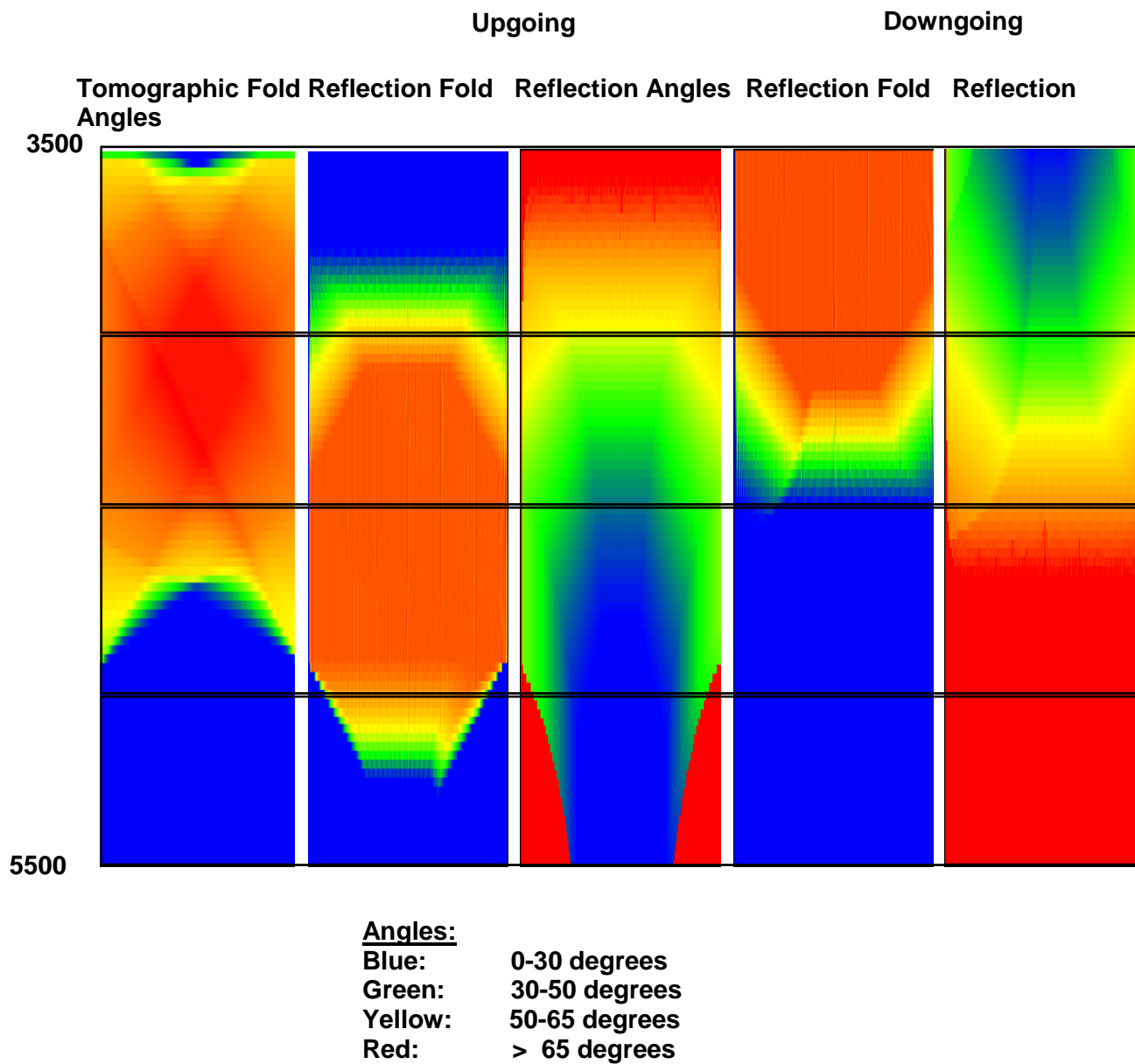


Figure 4. Angular coverage and fold charts.

level spacing of 5 feet is often used. The shooting chart, level spacing and a variety of other shooting parameters given in Table 1 selected specifically for the application, determine the production rate for acquisition and ultimately the operating time for the profile. Combining the results of coverage and the production rate model results in the optimum survey design that is updated as required based on signal quality observed in the field.

Table 1. Typical Acquisition Parameters

Well Spacing	Telemetry operating mode	Turn time between fans
Source type	Level spacing	Rig-up/rig-down time
Sweep length	Telemetry data rate	Shooting geometry
Smear distance	Sample period	Receiver spacing
Number of sweeps per level	Converter precision	Number of receiver levels
Source duty factor	Listen time	

Data Acquisition

The large volume of data required for accurate imaging of the interwell region requires specialized hardware and logging techniques to make crosswell logging cost effective. Z-Seis operates reliable and cost-effective, wireline-conveyed piezoelectric source and receiver tools, using a technique known as “shooting on-the-fly” shown in Figure 5. The multiple-level receiver string is positioned in the receiver wellbore. The source is operated while in motion and makes a traverse through the selected logging interval past the receivers. The receivers are then moved to the next position (or fan) in the acquisition plan and the source is again scanned by the receivers. Each fan that is acquired produces several common receiver gathers that are correlated and quality control checked on site to assure that adequate data are recorded to achieve project objectives. Current Z-Seis crosswell logging tools are described in Figure 6.

Crosswell operations described in Figure 7 draw heavily upon production logging methods. In many cases packoffs, lubricators or grease-injection equipment are required to meet pressure control requirements in the field. Gamma logs are used to tie-in the crosswell logging depths to original openhole logging depths so that all logging information for the well, including crosswell data, are on a common depth system. Gyroscopic deviation surveys and accurate wellhead locations are required to accurately place the information within a high-resolution crosswell image. Sonic and density logs are needed on one or more wells in a crosswell project to provide an accurate tie of crosswell seismic data to well logs using synthetic seismograms.

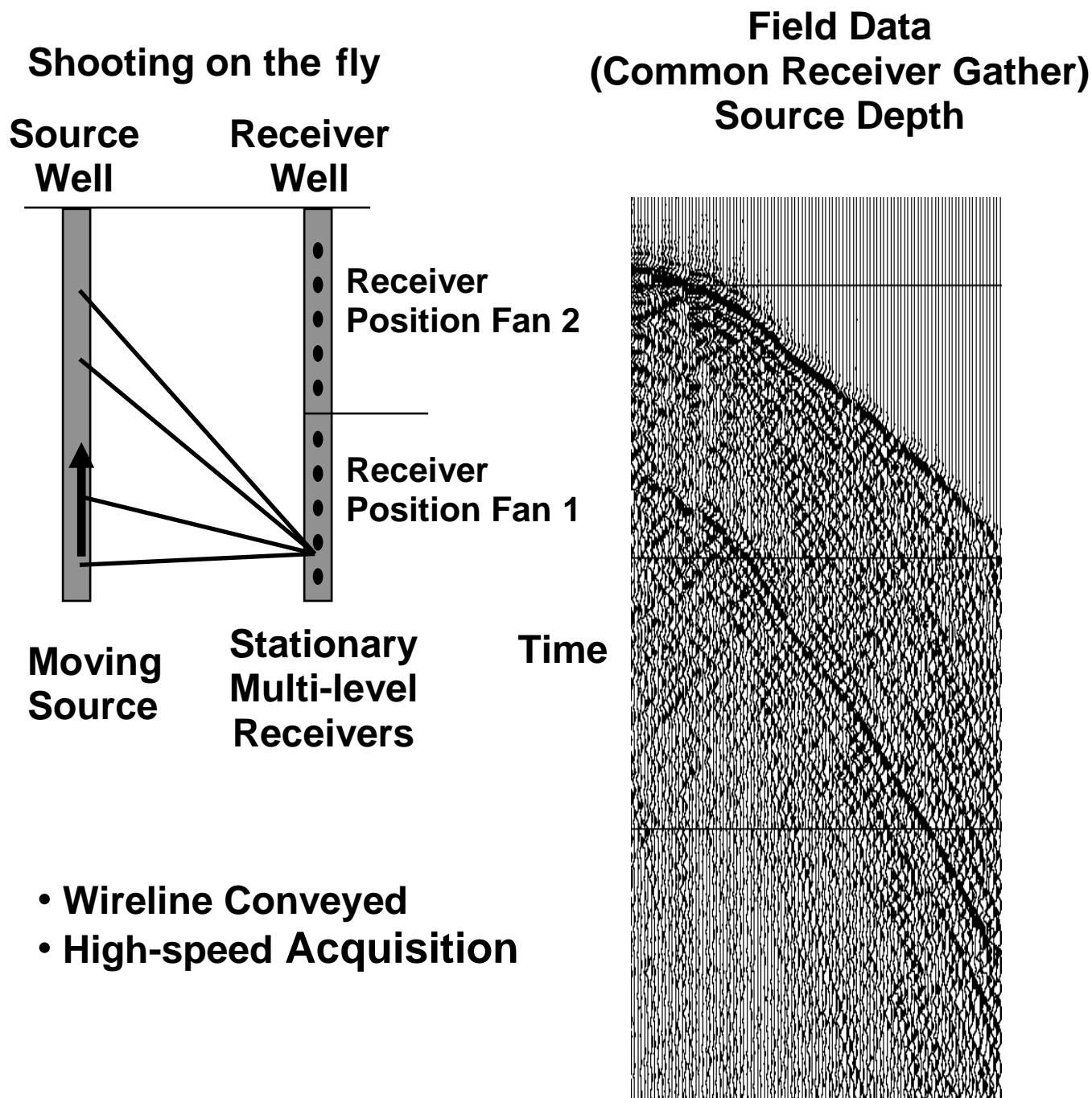


Figure 5. Crosswell seismic logging.

Source Technology

TomoSeis crosswell energy sources use piezoelectric technology, producing small displacements of the borehole fluid to apply energy over a large surface area in the wellbore. Extensive experience in over 50 cased wellbores has resulted in no evidence of damage to casing or cement. Because the source is not clamped to the wellbore, data can be rapidly logged with the source in constant motion.

Receiver Technology

TomoSeis receiver systems are built to withstand the rigors of the production well environment and to operate in vertical and deviated wells, both open and cased holes. The system is designed to operate within most production tubing. Several well pairs can be logged simultaneously with receiver systems operated in multiple wellbores around a single source well.

RCP Source



500 SLS Source



TomoSeis Analog Receiver System



Specifications:

Sources		Receivers	
RCP		Sensor type:	hydrophone
Source type:	piezoelectric	Level spacing:	5 feet
Length:	12.9 feet	Length:	37 feet
Diameter:	4.125 inches	Diameter:	1.7 inches
Duty cycle:	greater than 50 percent	Converter precision:	16 bits
Frequency range:	200 to 4,000 Hz	System bandwidth:	150 to 4,000 Hz
Source waveform:	programmable		
		System	
500 SLS		Operation:	cased or openhole operation
Source type:	piezoelectric	Tool conveyance:	wireline
Length:	4 feet	Maximum hole size:	26 inch
Diameter:	3.625 inches	Wireline tools:	H2S, CO2 resistant
Duty cycle:	greater than 50 percent	Depth:	greater than 15,000 feet
Frequency range:	500 to 4,000 Hz	Well conditions:	fluid filled (fluid can be added above removable bridge plug)
Source waveform:	programmable	Operating temperature:	125 degrees C (260 degrees F)
		Survey time:	12 to 48 hours, typical

Figure 6. TomoSeis crosswell logging tools.

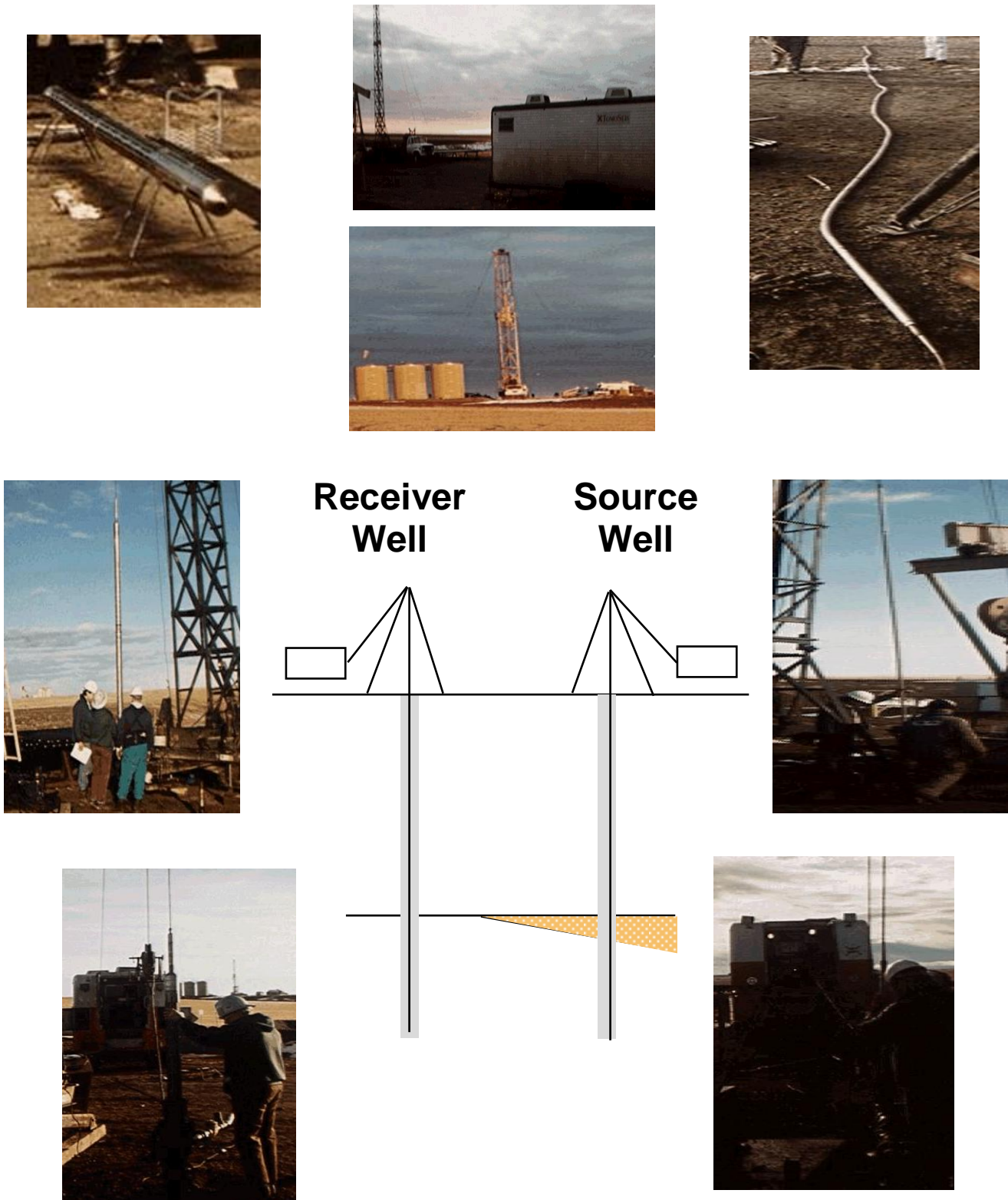
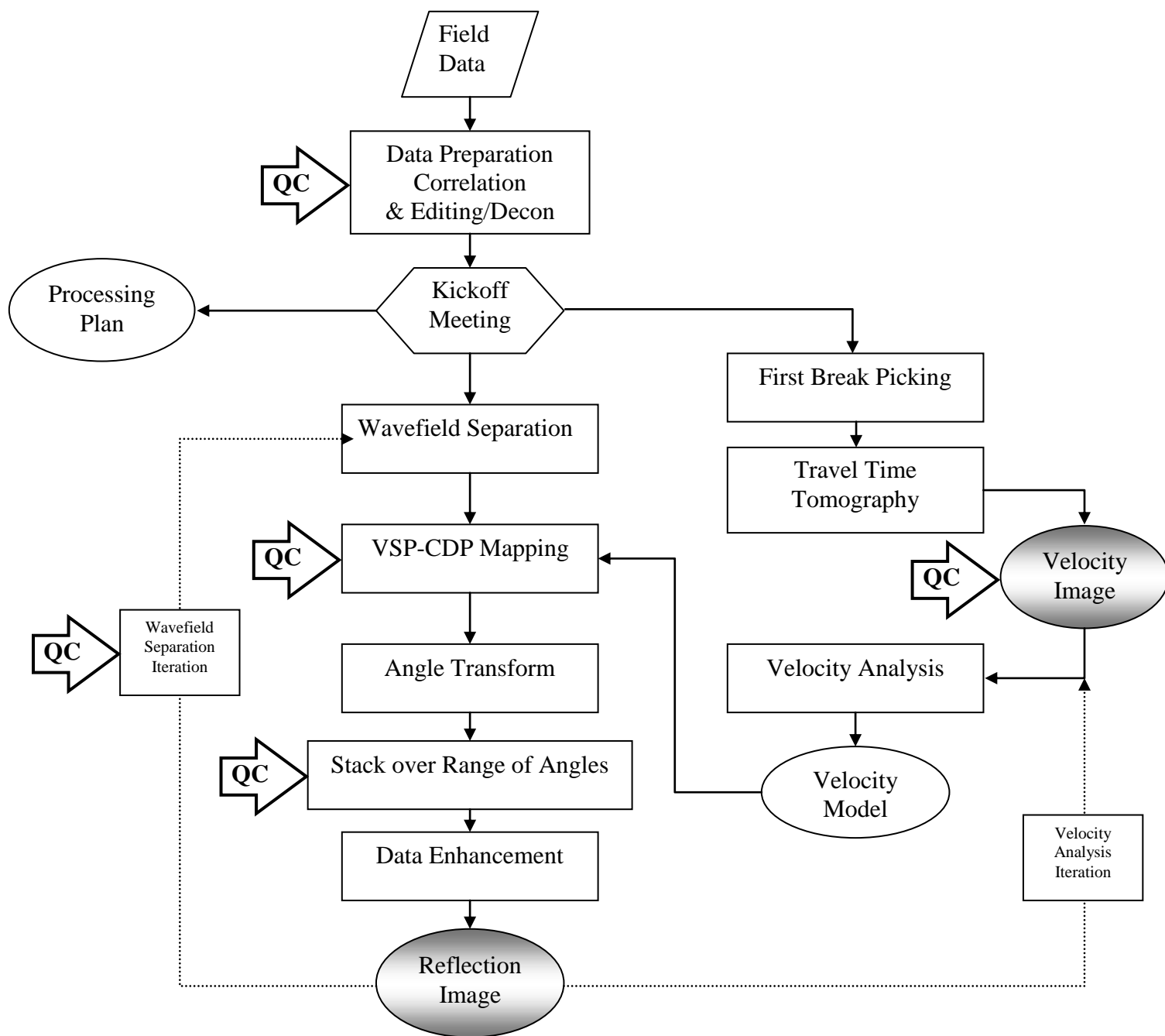


Figure 7. Crosswell operations.

Data Processing

We use methods from surface seismic and vertical seismic profiling (VSP) data processing to process crosswell seismic data. An overview of crosswell data processing is shown in Figure 8. Field records for swept-source acquisition are cross-correlated with a reference sweep and the data is edited and organized into a crosswell data set. The direct arrival traveltimes are measured in first-break picking to provide input for the traveltime tomographic inversion. The result is a velocity image between wellbores. The initial velocity image from traveltime tomography is a starting point for velocity analysis to produce a velocity model for the VSP-CDP mapping operation. Mapping transforms wavefield-separated data from a time-domain representation to a depth-domain reflection image. Wavefield separation, as in VSP processing, is used to separate other coherent arrivals present in the data from the primary reflection events needed in the mapped image. To produce interpretable images we sort the mapped data by reflection incidence angles and stacked over limited ranges of angles. The resulting stacks are enhanced and displayed. Two major iterations in processing are applied:

- For a given velocity model, wavefield separation parameters are updated to remove progressively more coherent events other than reflections that have survived in the angle-limited stack
- For a given wavefield-separated input data set, velocity analysis is performed to update the mapping velocity model and produce improved stack quality and coherence of reflection events in the angle-limited stack.

**Figure 8. Data Processing**

Interpretation

Interpretation of crosswell seismic data is similar to surface seismic interpretation when the differences in recording geometry and resolution are accommodated. A unique characteristic of crosswell data is the wide range of incidence angles available when compared with surface seismic or VSP. A synthetic seismogram produced from sonic and density logs, showing the change in response as a function of incidence angle is shown in Figure 9. Angle-limited stacks over several ranges of angles assist in separating angular effects. The importance of non-vertical incidence synthetic seismograms to tie crosswell to well logs is also demonstrated by the large changes in response as a function of angle in Figure 9.

Synthetic data sets modeling the features of interest are an essential step in understanding the response of crosswell acquisition and processing to the earth features. Such modeling serves to adapt surface seismic interpretation to the crosswell scale.

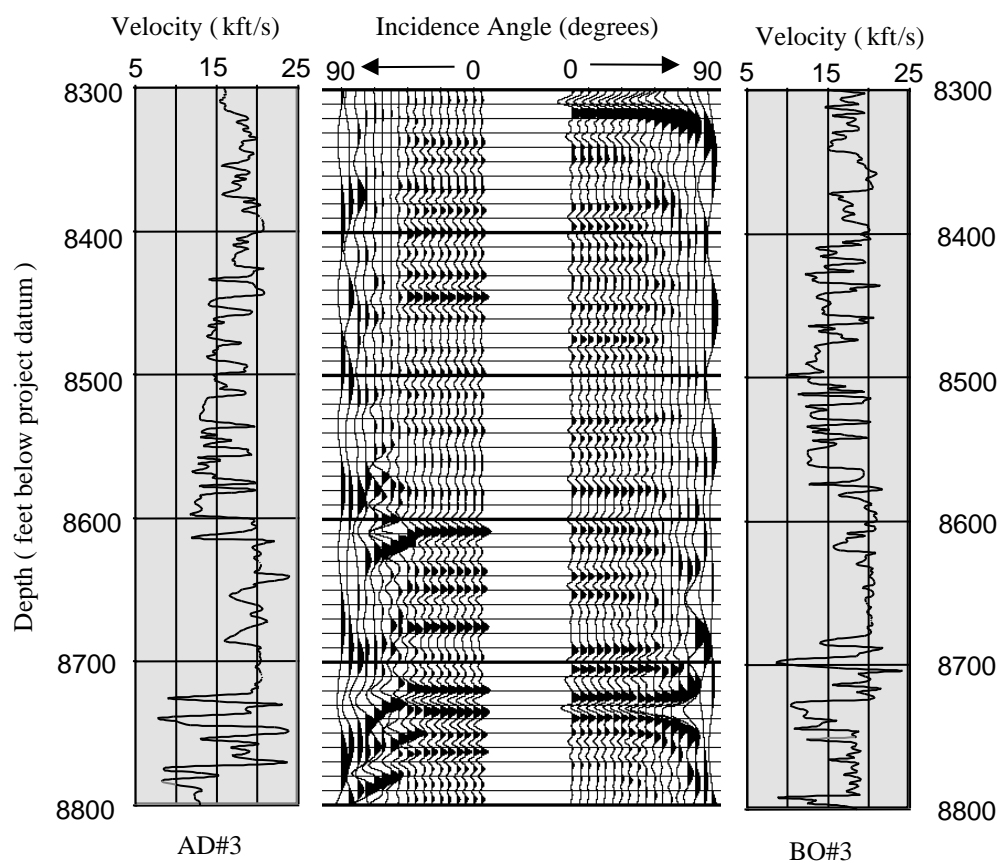


Figure 9. Interpretation

Glossary of Crosswell Terms

The glossary contains terminology unique to crosswell seismic technology or with a meaning unique to the crosswell application. Words in *italics* refer to another entry that supplements in effect the meaning. **Boldface** within an entry indicates additional terms defined herein. Terms commonly used in geophysics, wireline logging or other oilfield applications are not repeated in the glossary. Useful references for such terms include:

Sheriff, R.E., *Encyclopedic Dictionary of Exploration Geophysics*, Society of Exploration Geophysicists.

angle of incidence: When used to describe data from the *mapped cube*, the angle of incidence from the vertical at a reflection interface as shown in Figure G.1.

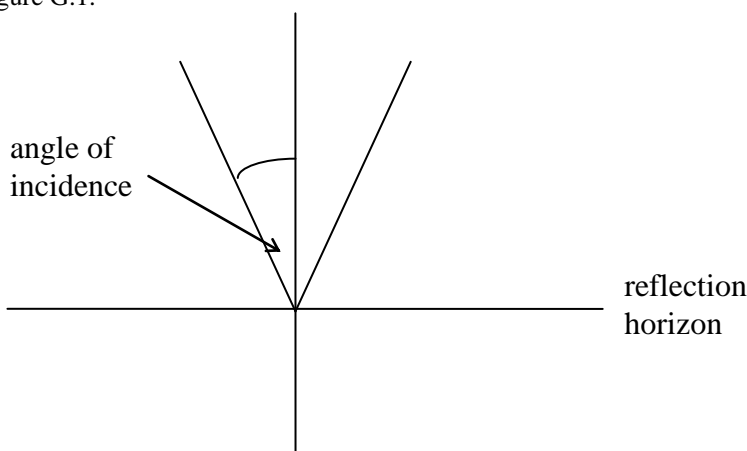


Figure G.1. Incidence angle.

angle-limited stack: A gather representing depth and distance between the wells formed by stacking the mapped data cube, including only data values whose *angle* falls within a specified, limited range.

angle transform: An algorithm for assigning an angle value to each element of the *mapped data cube*. Two common implementations are the straight-ray angle transform, assuming rays from source to reflection point and reflection point to receiver are straight, and the true angle transform, based on ray-theoretic propagation through the earth.

conversion: *P*-waves or *S*-waves can convert at an impedance boundary to another wave mode and propagate the remaining distance in that wave mode (or potentially convert again at another interface). Examples include *P-S* conversions, *S-P* conversions and *P-S-P* conversions. Both direct and reflected arrivals can undergo conversion.

common mid-depth gather (CMD): A gather sorted from the *time-domain data cube* containing traces from all source levels corresponding to the common mid-depth value. The common mid-depth gather places reflection events into similar times for each trace (depending on the velocity function) and represents reflection events within the logging interval from well to well. These attributes make the common mid-depth gather the preferred sort for the *time-domain data cube* prior to mapping. The coverage on a given reflection event provided by a common mid-depth gather is shown in Figure G.2.

common offset gather (COG): A gather sorted from the *time-domain data cube* containing traces from all source levels corresponding to the common offset value. See Figure G.3(c). In common offset gathers the direct arrival occurs at similar times for each trace (depending on the velocity function).

common receiver gather (CRG): A gather sorted from the *time-domain data cube* containing traces from all source levels corresponding to the common receiver value. See Figure G.3(a). In *shooting on-the-fly* with moving source, the CRG is the native data gather.

common source gather (CSG): A gather sorted from the *time-domain data cube* containing traces from all receiver levels corresponding to the common source value. See Figure G.3(b).

dead time: The time between the end of a sweep and the beginning of the next sweep for swept-source, stacked crosswell data acquisition.

direct P-wave: A compressional wave (*P*-wave) traveling along the direct path from source to receiver. See Figure G.4.

direct S-wave: A shear wave (*S*-wave) traveling along the direct path from source to receiver. See Figure G.4.

fan: A unit of measure used in data acquisition: the data acquired in one pass of one tool, typically the source by the other tool, typically multiple receivers. If a fan is collected scanning the source by a 10-level receiver system, the fan consists of 10 *common receiver gathers*.

mapped data cube: A 3-dimensional data volume, generally sampled along the 3 axes, in which crosswell data from a single profile are represented. This cube consists of data following *mapping* with the axes: depth, horizontal distance between wells, and a third parameter typically mid-depth depending on the sort applied to the time-domain cube prior to *mapping*.

mapping. Transformation from the *time-domain data cube* to the *mapped data cube* generally using the Vertical Seismic Profiling Common Depth Point (VSP-CDP) transformation (see Hardage, **Vertical Seismic Profiling, Part A: Principles**, Geophysical Press).

multiple: a wave mode with the same moveout as a primary *P*-wave (or *S*-wave) in a gather. The time delay between the primary and multiple corresponds to propagation through an additional path. See Figure G.4.

offset: Vertical offset -- difference in depth -- between the source and receiver for a trace in the *time-domain data cube*.

pick map: A display of the direct-arrival traveltimes in a *shooting chart*, where color values are used to display the traveltime values as shown in Figure G.5.

primary P-reflection. A compressional wave that travels from the source, reflects as a compressional wave at a reflection horizon and travels to the receiver. See Figure G.4.

primary S-reflection. A shear wave that travels from the source, reflects as a shear wave at a reflection horizon and travels to the receiver. See Figure G.4.

profile: A crosswell survey conducted between a single pair of wellbores.

shooting chart: A display of an attribute of a crosswell data set for a profile as in Figure G.6 where the vertical axis is source depth and the horizontal axis is receiver depth. A binary-valued shooting chart indicates the levels at which a trace was shot in a crosswell data set.

shooting on-the-fly: Crosswell data acquisition in which data is acquired while one tool, typically the source, is in motion. Shooting on-the-fly provides more rapid, cost-effective acquisition with the penalty of introducing *smear* into the data.

smear distance: The distance traversed by the source in stacked, multi-shot or multi-sweep crosswell *shooting on-the-fly*. The total smear may also refer to the effective total distance including the active tool length and the distance traversed.

time-domain data cube: A 3-dimensional data volume, generally sampled along the 3 axes, in which crosswell data from a single profile are represented. This cube consists of data positioned as acquired with the axes: source depth, receiver depth and time. If a correlative source is used, the time-domain cube generally consists of correlated data: for impulsive sources the cube represents time as recorded. The time-domain cube can be sorted into 4 gathers: *common receiver*, *common source*, *common offset* and *common mid-depth*.

tube wave: A fluid-borne interface wave propagating in a borehole. "Tube wave" arrivals identified in crosswell records propagate as a tube wave for some distance in the source well, the receiver well or both and convert at a borehole interface to or from a body wave that propagates between the wellbores. See Figure G.4.

1.5-D: Designates a 2-dimensional model, typically of velocity, that allows only planar, non-truncating dips.

2-D: Designates a 2-dimensional model, typically of velocity that allows arbitrary 2-dimensional variation in the modeled parameter.

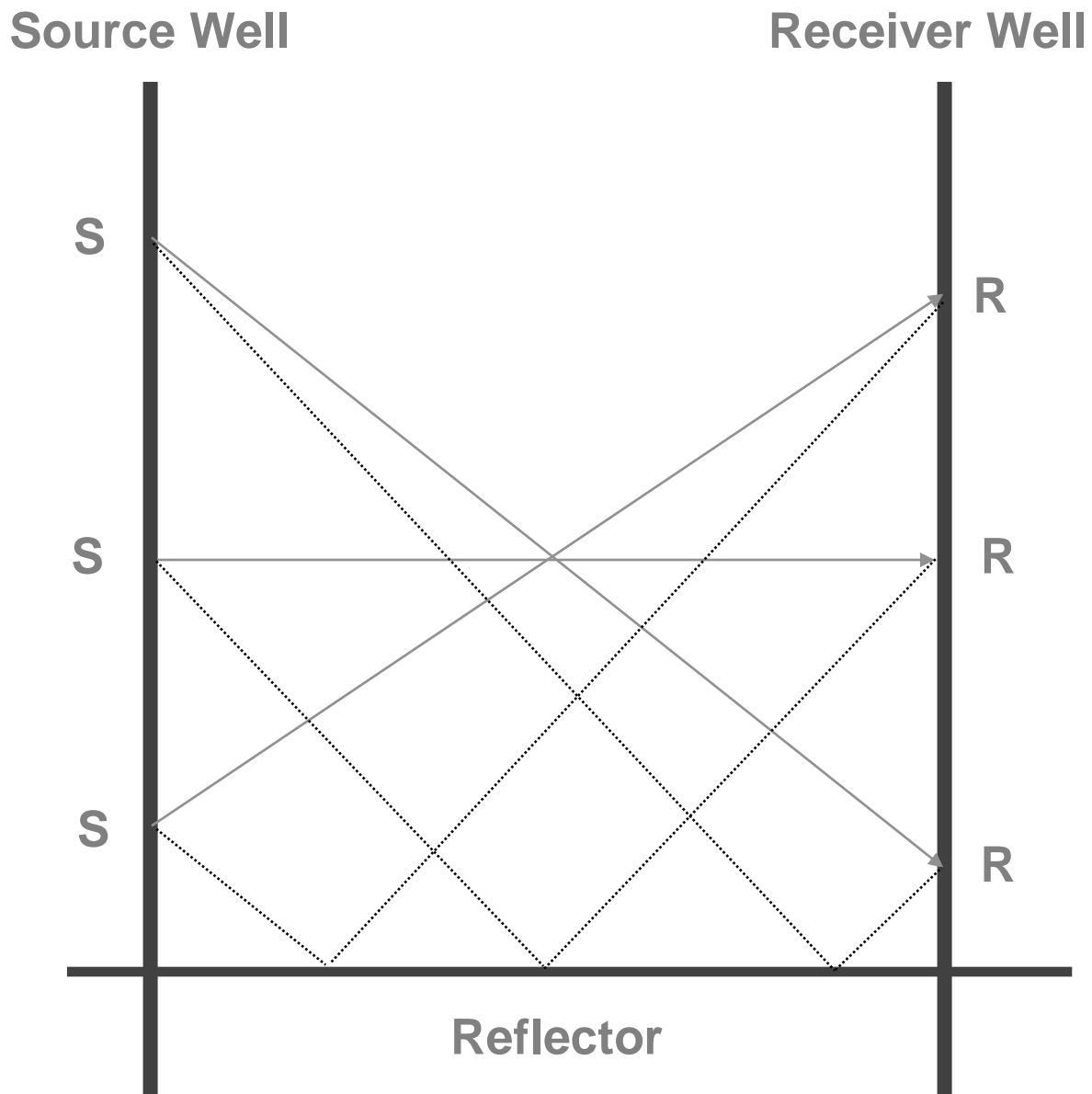
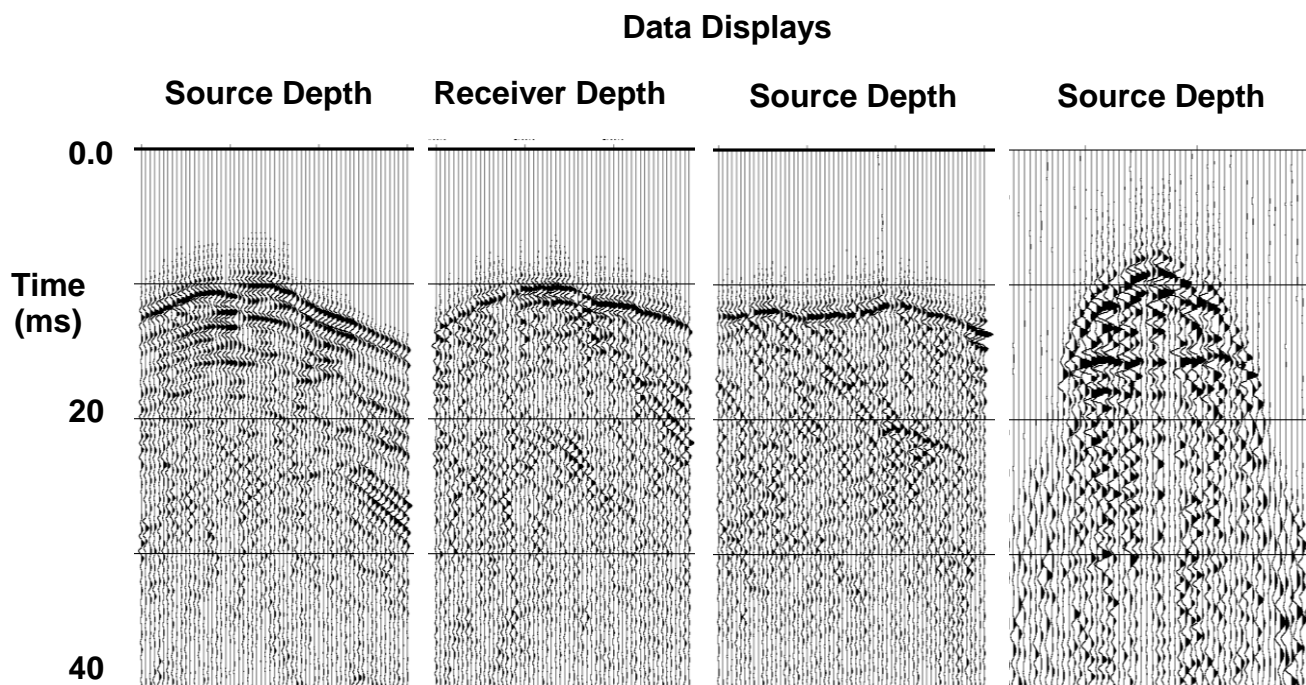


Figure G.2. Common mid-depth gather.



(a) Common Receiver (b) Common Source (c) Common Offset (d) Common Mid-Depth

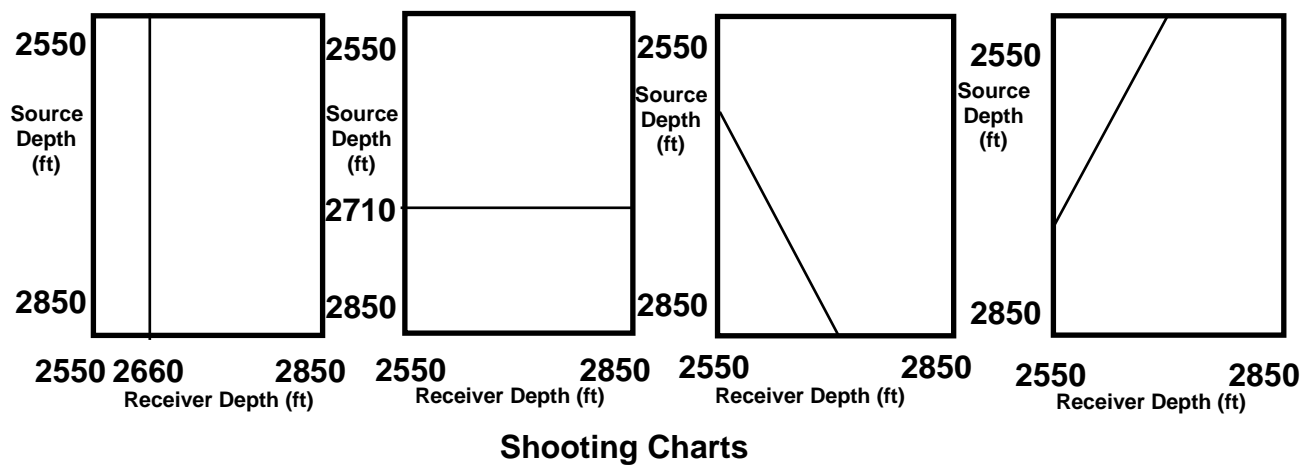


Figure G.3. 4 crosswell data displays from the time-domain data cube.

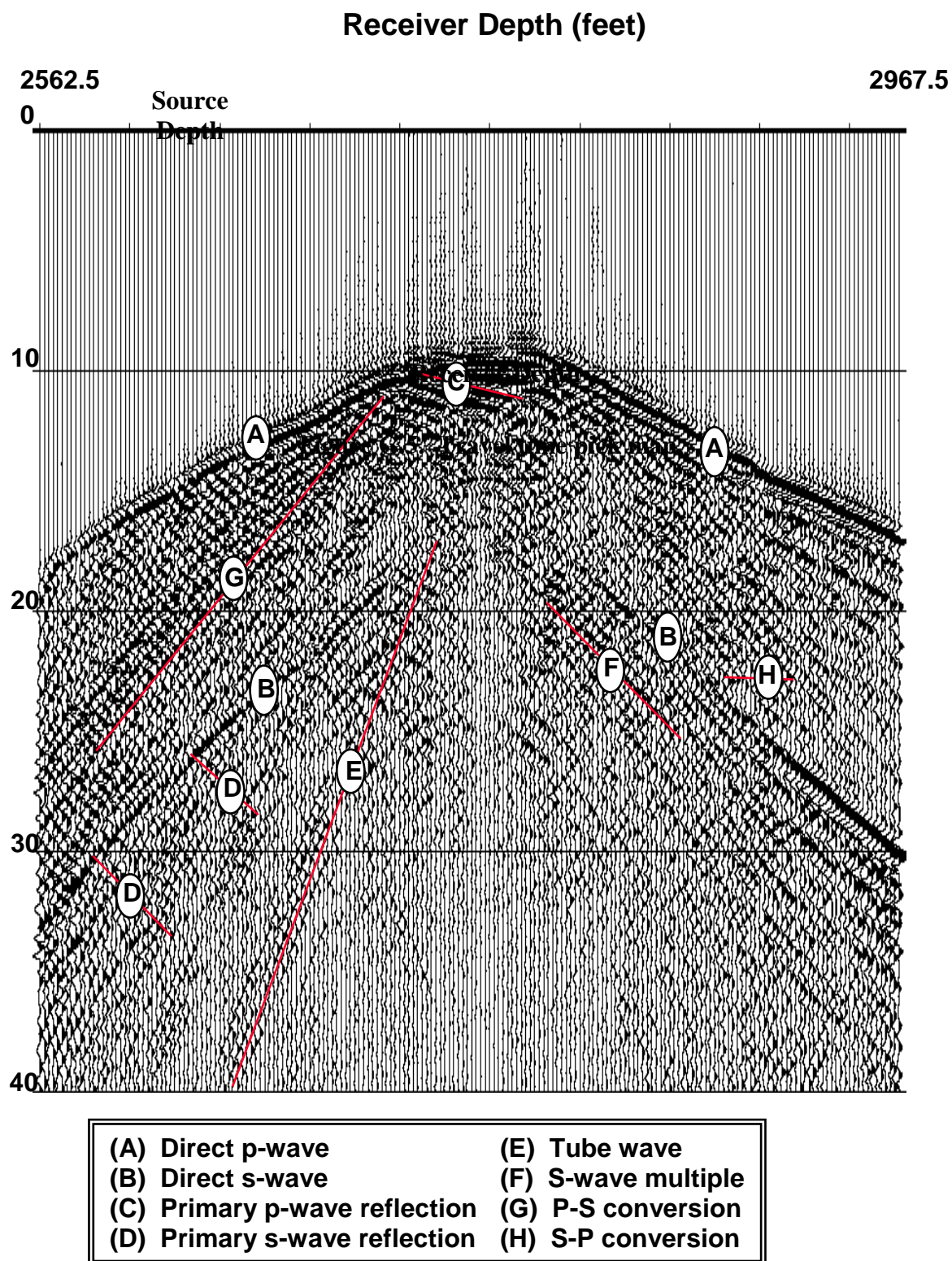


Figure G.4. Arrivals identified in a crosswell common source gather.

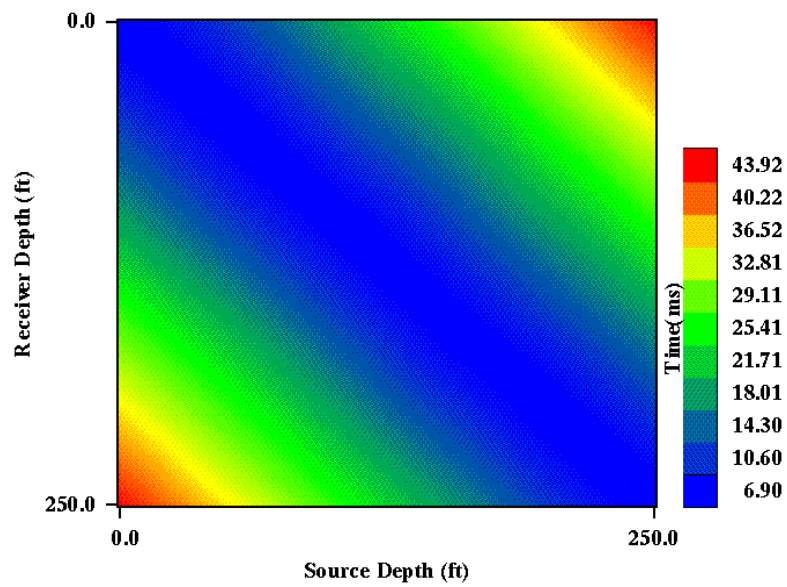


Figure G.5. Travel time pick map.

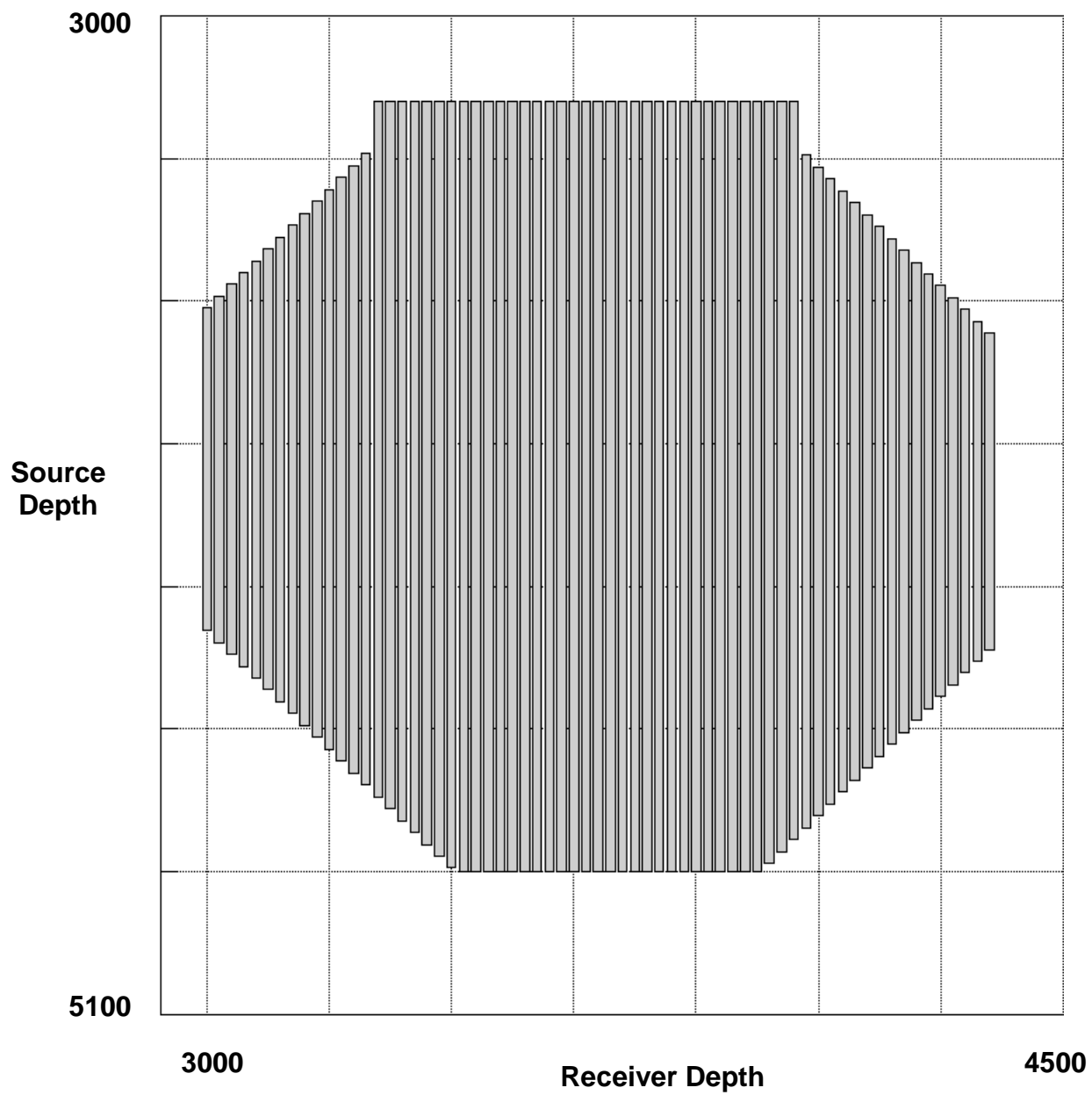


Figure G.6. Crosswell shooting chart

ENCLOSURES